Int J Adv Manuf Technol (2017) 92:2341–2363
DOI 10.1007/s00170-017-0279-0

ORIGINAL ARTICLE

Computational analysis of turning G10530 steel to eliminate chip crowding using variable cutting speeds

Mark J. Jackson[1,2,3] · **Edward Lathery**[1] · **Michael D. Whitfield**[1] · **Rod G. Handy**[1] · **Marcio Bacci da Silva**[2] · **Alisson R. Machado**[2,4] · **Rosemar B. da Silva**[5]

Received: 4 December 2016 / Accepted: 9 March 2017 / Published online: 31 March 2017

Abstract The machining of axle hub flange housings manufactured using G10530 steel is described in this paper. The machining of axle hub flange housings can lead to the entanglement of chips around workpiece holding fixtures, which leads to a loss of productivity due to the interruption of the machining process to remove entangled machining chips in the vicinity of the chuck (chip crowding). The finite element (FE) method was used to predict machining characteristics in order to eliminate the phenomenon of 'chip crowding' around rotating machine parts that impede the effective machining of axle hub flange housings. The finite element method is compared to traditional analytical calculations to observe whether discrete computations can accurately predict machining characteristics and to visually predict the shape of chips to eliminate the possibility of 'chip crowding'. From this study, it is shown that short chips can be created using variable cutting speeds and that the FE method can be used to analyze chip formations in order to optimize the turning of G10530 axle hub flange housings. For the current practice of machining axle hub housings, when f_{edge}/t_r = 0.25 (small cutting edge radius), the level of power required for chip formation is calculated to be 6400 W generating a maximum temperature at the onset of chip formation of ~563 °C, and when f_{edge}/t_r = 0.75 (large cutting edge radius), the level of power required for chip formation is calculated to be 3200 W generating a maximum temperature at the onset of chip formation of ~292 °C. When forming chips at variable cutting speeds, the best case condition is one that draws the least power and generates the lowest temperature at the chip tool interface. This is achieved when a large cutting edge radius tool (f_{edge}/t_r = 0.75) is used for machining axle hub flanges. Closed form solutions appear to describe the machining conditions at the steady-state conditions very accurately. However, the FE method tends to generate accurate values under the conditions of unsteady chip formation when cutting at variable speeds. The innovations presented in this paper are associated with providing the necessary information to machine axle hub flanges with variable cutting speeds that eliminate the occurrence of 'chip crowding' by naturally fragmenting the formation of long metal chips.

Keywords Computation · Finite elements · Machining · Steel · Manufacturing

✉ Mark J. Jackson
jacksonmj04@yahoo.com; mjjackson@k-state.edu

[1] Center for Advanced Manufacturing, Purdue University, Lafayette, IN, USA

[2] LEPU/FEMEC, Federal University of Uberlandia, Uberlândia, MG 38.400-902, Brazil

[3] Present address: Kansas State University, Manhattan,, KS, USA

[4] Mechanical Engineering Graduate Program, Pontifícia Universidade Católica do Paraná (PUC-PR), Curitiba, PR 80215-901, Brazil

[5] School of Mechanical Engineering, Federal University of Uberlandia, Av. João Naves de Ávila, 2121, Uberlandia, MG 38408-100, Brazil

1 Introduction

Hub flanges are an essential component of the axle assembly in automotive vehicles. The hub flange has internal and external parts associated with it, and for these reasons, close tolerances are required from machined hub flanges. The internal parts are composed of the inner cup, inner bearing, and double lip seal, whereas the external parts are composed of the outer cup, outer bearing, castle nut, pin, retaining washer, and the dust cap. Figure 1 shows a typical hub flange with a machined

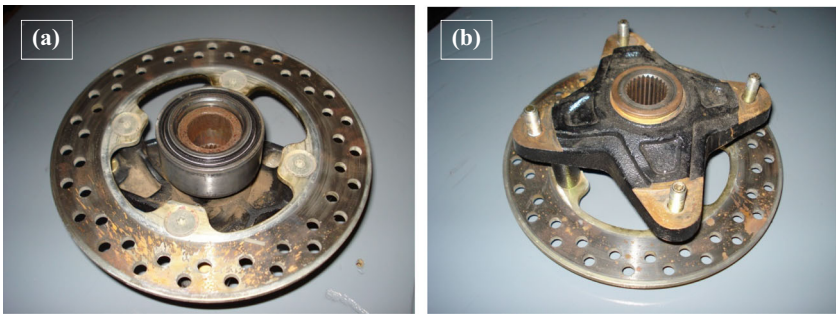

Fig. 1 Heavily used axle hub flanges made from UNS G10530 steel showing **a** machined bearing surfaces plus double lip seal, inner bearings, and inner cup; and **b** machined and assembled hub flange with studs

bearing surface and associated bearings, inner cup, and double lip seal. Prior to the extensive use of machining centers, turret lathes were used to machine hub flanges using primary and secondary tools for rough turning and finish turning of hub flanges and differential gear housings. There is surprisingly little published in articles about the machining of hub flanges, although one publication described by Yeoman in 1922 [1] discusses the machining of hub flanges using turret tooling. The first part of Yeoman's article focused on rough turning operations for gear housings, and his work shows the type of operations used to size the housings for the final finish machining operations. Although no machining parameters were provided, it was shown that the purpose of rough machining is to produce the bulk of the machining chips so that they can be cleared away prior to machining the final tolerances on the part. Here, it is assumed that condition of the tools is designed for high material removal with rake and clearance angles that are designed for turning large chips that can be cleared away after they have been created. For the finish operation, the tools appeared to have less acute angles so that thin chips can be generated at much smaller feed rates than those in rough turning. From the images shown in reference [1], chips were allowed to crowd the area between tool and workpiece. To support the need for analyzing actual production machining for specific mechanical components, there is a growing trend of analyzing production machining processes in various industries and industrial sectors. For example, academic researchers recently analyzed the effect of using re-ground machining inserts to machine hardened steels [2], optimizing of cutting conditions using genetic algorithms for aerospace components [3], analyzing the use of modulated tool path machining to control residual surface stresses when machining precision bearing surfaces [4], defining the effects of coolant concentration on the surface features generated in micromilled MEMS components [5] and minimizing the height of burr milling precipitation hardened steels using surface response methodologies [6].

The purpose of this paper is to show how using variable cutting speeds can avoid the phenomena known as 'chip crowding' because chips accumulate owing to the generation of one long chip that subsequently entangles the chuck and associated workpiece holding fixtures. These chips are unacceptable in a production environment as they tend to have an adverse effect on operator safety, surface finish, tool breakage, and disposal. This phenomenon is common when using a single cutting speed even for multiple operations on the same component.

The following sections of the paper explain how the finite element method and a constitutive material model are used in formulating the simulation of industrial machining conditions associated with the machining of axle hub flanges manufactured from G10530 steel. The conditions of turning of a particular hub flange will be explained in terms of chip formation and the effects of changing cutting speeds, feeds, and depths of cut. The simulations not only show how machining parameters affect the conditions of machining axle hub flanges, but will also focus on what happens when a different tool is used in the rough machining operation to eliminate the possibility of 'chip crowding'.

2 Computational analysis

2.1 Finite element model

The model used in the computational analysis of axle hub flanges is a three-dimensional Lagrangian-Eulerian formulated finite element model explicitly dynamic that is thermo-mechanically coupled. The model uses adaptive re-meshing that is capable of finite spatial resolutions to incorporate cutting edge radii, primary and secondary shear zones, and chip loading phenomena. Multiple body deformations simulate tool-workpiece interactions and transient thermal consequences. Finite deformation kinematics and improvised stress conditions have been formulated by Third Wave Systems in their commercially available software package known as 'AdvantEdge™' that includes balancing linear momentum and calculating the associated thermal conditions using the second law of thermodynamics [7–14]. For brevity, the following conditions are described so that readers who are not proficient in the use of finite elements for analyzing hub flange machining operations are aware of the mathematical procedures necessary to assess the effects of machining conditions on chip crowding.

For dynamic kinematic conditions [14], the balance of linear momentum is as follows:

$$\sigma_{ij,j} + \rho b_i = \rho \ddot{u}_i \tag{1}$$

The principle of virtual work in its weakest form is as follows:

$$\int_B v_i \sigma_{ij,j} + v_i \rho b_i dV = \int_B \rho v_i \ddot{u}_i dV \tag{2}$$

Integrating Eq. 2 by parts and re-arranging the terms provide the force balance for the machining system:

$$\int_B \rho v_i \ddot{u}_i dV + \int_B v_{i,j} \sigma_{i,j} dV = \int_{\partial B} v_i \sigma_{i,j} n_j d\Omega + \int_B v_i \rho b_i dV \tag{3}$$

Hence, (inertial terms) + (internal forces) = (external forces) + (body forces).

In matrix format, the force balance becomes the following:

$$\boldsymbol{M a}_{a+1} + \boldsymbol{R}^{int}_{n+1} = \boldsymbol{R}^{ext}_{n+1} \tag{4}$$

Where,

$$M_{ab} = \int_{B0} \rho_0 N_a N_b dV_o \tag{5}$$

Here, M_{ab} is the mass matrix and the external force array, R_{ia}, is

$$R^{ext}_{ia} = \int_{B0} b_i N_a dV_o + \int_{\partial B0\tau} \tau_i N_a d\Omega_o \tag{6}$$

And the internal force array is simply

$$R^{int}_{ia} = \int_{BO} P_{i,j} N_{a,j} dV_o \tag{7}$$

It should be noted that N_a, a = 1…..n,u,m,p are the shape functions, and that repeated indices imply summation. A comma (,) represents a partial differentiation with respect to the spatial coordinate, and $P_{i,j}$ is the nominal stress known as the 'Piola-Kirchhoff' stress tensor.

For dynamic thermal conditions [14], heat generation and transfer are derived using the second law of thermodynamics. A weak form of the first law of thermodynamics in discretized form is as follows:

$$\boldsymbol{C}\dot{\boldsymbol{T}}_{\boldsymbol{n}+1} + \boldsymbol{K}\boldsymbol{T}_{\boldsymbol{n}+1} = \boldsymbol{Q}_{\boldsymbol{n}+1} \tag{8}$$

A lumped capacitance matrix, **C**, is used to eliminate the need for solving equations:

$$\boldsymbol{C}\,\dot{\boldsymbol{T}} + \boldsymbol{K}\boldsymbol{T} = \boldsymbol{Q} \tag{9}$$

where **T** is the array of temperature nodes and the heat capacity matrix is as follows:

$$C_{ab} = \int_{Bt} c\rho N_a N_b dV_o \tag{10}$$

The heat conductivity matrix is

$$K_{ab} = \int_{B0} D_{i,j} N_{a,i} N_{b,j} dV \tag{11}$$

The heat source array assumes that the chip, or tool, has the appropriate value of h:

$$Q_a = \int_{Bt} s N_a dV + \int_{B\tau q} h N_a dS \tag{12}$$

During machining processes, the sources of heat generation are from the formation of chips due to plastic deformation and frictional sliding of the chip at the tool-workpiece interface. The rate of heat generated is as follows:

$$s = \beta . W^p \tag{13}$$

where $\dot{W}^p$ is the power consumed in plastic deformation per unit deformed volume and the Taylor-Quinney coefficient, β, is less than unity (β ~ 0.9). The rate of heat generated by the chip at the frictional contact zone is

$$h = -\boldsymbol{t}.\|\boldsymbol{v}\| \tag{14}$$

where **t** is the traction at the contact zone and **v** is the velocity across the contact zone. A full description of the mathematical formulation of the FE method with explanations of the symbols used and assumptions made in the model can be found in the manual that accompanies the AdvantEdge™ software package [14].

In order to use the finite element model to simulate the conditions of machining axle hub flanges, an appropriate material model is required to properly simulate machining conditions by knowing the condition of the workpiece material. For this reason, a customized power law constitutive material model was employed. The next section of the paper describes the types of constitutive models available and the methods employed to select the appropriate model for the analysis of machining axle hub flanges.

2.2 Constitutive material models

Manufacturing processes such as machining and forming introduce large deformations with various stress, strain, and temperature levels creating complex deformation states. Material flow stresses in manufacturing processes are also influenced by strain rate, loading history as well as thermal history. The size effect in machining is incorporated in the material models by modeling the material strengthening mechanism. Many models have been developed, but no model has been proven to correctly describe the behavior of all materials used in the vast number of processes in manufacturing practice.

2.2.1 Johnson-Cook model[7]

Johnson-Cook (J-C) model represents a phenomenological material model most often used in literature for finite element analysis (FEA) and modeling of material behavior [7]. It is most often used with the aim to show the dependence of the flow stress on strain rate and temperature. The mathematical representation of the J-C model is presented with the following equations [8]:

$$\sigma = (A + B\varepsilon^n)\left[1 + C\ln\frac{\dot{\varepsilon}}{\dot{\varepsilon}_0}\right](1-T_h{}^m) \tag{15}$$

$$T_h = (T-T_{\text{room}})\Big/(T_{\text{melt}}-T_{\text{room}}) \tag{16}$$

where ε is the equivalent plastic strain, $\dot{\varepsilon}$ is the strain rate, $\dot{\varepsilon}_0$ is the reference strain rate, and the constants are as follows: A is the yield strength of the material, B and n represent the strain hardening, C is the strain rate constant, T_h is the homologous temperature, T_{melt} is the melting temperature, and T_{room} is the room temperature.

There have been several modifications of the J-C model described in the literature regarding the temperature parameter that accounts for the effect of temperature before and after the recrystallization temperature has been reached, a modification of the model with the aim of accounting for the strain softening effect, and a modification to the model using the 'Arrhenius' exponential approach to material behavior with respect to the temperature, rather than the linear dependence of temperature to represent the effects of adiabatic plasticity [9–16].

The mathematical formulation of the modified J-C model incorporating the effect of recrystallization temperature is presented as follows [10]:

$$\sigma = (A + B\varepsilon^n)\left[1 + C\left(\ln\frac{\dot{\varepsilon}}{\dot{\varepsilon}_0}\right)^m\right][1-(T_h)^m]\frac{(\sigma_f)_{def}}{(\sigma_f)_{rec}} \tag{17}$$

where $(\sigma_f)_{def}$ and $(\sigma_f)_{rec}$ represent the flow stress of the material prior to, and after, recrystallization. The ratio of flow stresses before and after reaching the recrystallization temperature has been introduced in order to account for phase transformations that are triggered by increasing the temperature above the recrystallization temperature that would undoubtedly influence material behavior.

The mathematical formulation of the modified J-C model incorporating the exponential term to more accurately determine Arrhenius-type dependence for adiabatic plasticity is as follows [11]:

$$\tau = [B\gamma^n]\left[1 + C\ln\left(\dot{\gamma}\Big/\dot{\gamma}_0\right)\right]f(\bar{T}) \tag{18}$$

$$\bar{T} = T_m - T\Big/T_m \tag{19}$$

where B, n, and C are the material constants, $\bar{T}$ is the dimensionless temperature, T_m is the melting temperature, T_0 is the reference temperature, and $\dot{\gamma}_0$ is the reference strain rate.

The exponential term that more accurately represents the adiabatic plasticity is as follows:

$$f(\bar{T}) = \left(\tau\Big/\tau_0\right)_{\gamma\dot{\gamma}} \tag{20}$$

where τ is the shear stress at a given T and τ_0 is the shear stress at a reference temperature.

The mathematical formulation of the modified J-C model incorporating not only the effect of strain rate hardening and thermal softening, but also strain softening (the (tan h) function shown in Eq. 21), is described by Eq. 21 [10]:

$$\sigma = \left(A + B\varepsilon^n\left(\frac{1}{\exp(\varepsilon^a)}\right)\right)\left(1 + C\ln\frac{\dot{\varepsilon}}{\dot{\varepsilon}_0}\right)\left(1-\left(\frac{T-T_r}{T_m-T_r}\right)^m\right)\left(D + (1-D)\tanh\left(\frac{1}{(\varepsilon+S)^c}\right)\right) \tag{21}$$

where functions D and S are as follows:

$$D = 1-\left(\frac{T}{T_m}\right)^d$$

$$S = \left(\frac{T}{Tm}\right)^b$$

where A, B, C, a, b, c, and d are the material constants, σ is the equivalent flow stress, ε is the equivalent plastic strain, $\dot{\varepsilon}$ is the strain rate, $\dot{\varepsilon}_0$ is the reference strain rate, T the workpiece temperature, and T_m and T_r are the material melting and room temperature values, respectively. This model shows a great influence on chip formation and chip shape due to the fact that strain softening has an effect on the appearance of shear localization enabling the formation of segmented chips. The predictions using this model are not satisfactory when the strain softening level is quite low.

The J-C model describes the material behavior relatively well. However, it is a model which does not incorporate the effect of the loading path, strain rate history, or temperature history, on the overall behavior of the material during machining. The J-C model uses the determination of constants from experimental data through curve fitting which has no validity if extrapolated beyond the available data. This makes the model inadequate for applications beyond deformation conditions and microstructures presented in the experimental data. This becomes a serious problem when dealing with machining processes in which deformation is significantly more severe than that achieved in standard deformation experiments used for material characterization purposes [8]. For these reasons, the J-C model is not used to assess the chip formation capabilities in hub flange turning operations.

2.2.2 Zerilli and Armstrong model [12]

The Zerilli and Armstrong model [12] represents a semi-empirical model based on dislocation mechanics with the aim of incorporating strain hardening and thermal softening effects into the material deformation model [12]. This model actually differentiates between face-centered crystals (FCC) and body-centered crystals (BCC) with the reasoning that the dislocation mechanism characteristics in BCC materials are not affected by temperature and strain rates while FCC crystals are affected by temperature [8].

The mathematical formulation of the Zerilli-Armstrong model for BCC and FCC crystals, respectively, can be presented as follows [12]:

$$\sigma = \Delta\sigma_G^{'} + C_1 \exp\left(-C_3 T + C_4 T \ln\dot{\varepsilon}\right) + C_5 \varepsilon^n + kl^{-1/2} \tag{22}$$

$$\sigma = \Delta\sigma_G^{'} + C_2 \varepsilon^{0.5} \exp\left(-C_3 T + C_4 T \ln\dot{\varepsilon}\right) + kl^{-1/2} \tag{23}$$

where $\Delta\sigma_G^{'}$ is the additional component of stress that is a result of the influence solute and the original dislocation density on yield stress, σ is the yield stress, ε is the strain, ε̇ is the strain rate, k is the microstructural stress intensity, l is the average grain diameter, and C_1–C_5 are material constants.

The model incorporates the thermal activation necessary in order to overcome obstacles for dislocation motion and dislocation interaction in materials. The dislocation mechanisms are considered to be different for different crystal lattices and are considered to be the cutting of dislocation concentrates in FCC metals and overcoming Peierls-Nabarro barriers in BCC metals. Therefore, the flow stress that incorporates the combined effects of temperature and strain rate is a function of yield stress in BCC metals and hardening stress in FCC metals [13]. Owing to its inherent complexity, this material model is not used to analyze chip formation capabilities in hub flange turning operations.

2.2.3 Bammann, Chiesa, and Johnson model[8]

The BCJ model represents an internal state variable plasticity model. The BCJ model takes into consideration temperature sensitivity, strain rate sensitivity, and the damage effects by incorporating hardening and recovery into the model by using the deformation path history effect. The model takes into account the rate of change of internal as well as observable state variables including the creep and plasticity through a deviatoric inelastic flow rule represented as a function of temperature, kinematic hardening internal state variable, isotropic hardening internal state variable, and the functions related to yielding with an Arrhenius-type temperature function [3]. The mathematical representation is presented as follows:

$$\overset{\circ}{\underline{\sigma}} = \dot{\underline{\sigma}} - \underline{W}^e \underline{\sigma} + \underline{\sigma}\,\underline{W}^e = \lambda tr\left(\underline{D}^e\right)\underline{I} + 2\mu\underline{D}^e \tag{24}$$

$$D^e = \underline{D} - \underline{D}^{\text{in}} \tag{25}$$

$$D^{\text{in}} = f(T)\sinh\left[\frac{\|\sigma_- - \alpha_-\| - \{R + Y(T)\}}{V(T)}\right]\frac{\sigma_- - \alpha_-}{\|\sigma_- - \alpha_-\|} \tag{26}$$

$$\overset{\circ}{\underline{\alpha}} = \dot{\underline{\alpha}} - W^e\alpha + \alpha W^e$$

$$= \left\{h(T)\underline{D}^{\text{in}} - \left[\sqrt{\frac{2}{3}} r_d(T)\left\|\underline{D}^{\text{in}}\right\| + r_s(T)\right]\left\|\underline{\alpha}\right\|\underline{\alpha}\right\} \tag{27}$$

$$\dot{R} = \left\{H(T)\underline{D}^{\text{in}} - \left[\sqrt{\frac{2}{3}} r_d(T)\left\|\underline{D}^{\text{in}}\right\| + R_s(T)\right]R^2\right\} \tag{28}$$

Where $\overset{\circ}{\underline{\sigma}}$ and α are the objective rates, W_-^e is the elastic spin, μ and λ are the elastic Lame constants, D_-^e is the elastic rate of deformation, D_- is the total rate of deformation, D_-^{in} is the inelastic rate of deformation, f(T) is the strain rate at which yield transition from rate-independent to rate-dependent, h(T) is the anisotropic hardening modulus, H(T) is the isotropic hardening modulus, Rd and r_d(T) represent the dynamic recovery, r_s(T) and R_s(T) represent diffusion-controlled static or thermal recovery, and α_- is the kinematic hardening internal state variable. Even though this model incorporates effects that have been neglected in other models, it has 20 constants that need to be determined for the calculations. Although a non-linear least squares' program exists for the determination of these constants, the process is still very complicated to compute.

2.2.4 Power law model [9]

In order to describe the material behavior, the material model that will be used in the finite element analysis (FEA) is a 'power law model' [14]. In order to correctly predict the behavior of the material during machining, strain hardening, strain rate sensitivity, thermal softening, and a damage model are included, thus:

$$\sigma\left(\varepsilon^p, \dot{\varepsilon}, T\right) = g(\varepsilon^p)^* \Gamma\left(\dot{\varepsilon}\right)^* \Theta(T) \tag{29}$$

where $g(\varepsilon^p)$ accounts for strain hardening, Γ (ε̇) for strain rate sensitivity, and Θ (t) for thermal softening. The strain hardening function is presented by the following:

$$g(\varepsilon^p) = \sigma_0\left[1 + \frac{\varepsilon^p}{\varepsilon_0^p}\right]^{\frac{1}{n}} \quad \text{if} \quad \varepsilon^p < \varepsilon_{cut}^p \tag{30}$$

$$g(\varepsilon^p) = \sigma_0\left[1 + \frac{\varepsilon_{cut}^p}{\varepsilon_0^p}\right]^{\frac{1}{n}} \quad if \quad \varepsilon^p \geq \varepsilon_{cut}^p \tag{31}$$

where σ_0 the initial yield stress, ε^p is the plastic strain, $\varepsilon_0{}^p$ is the reference plastic strain, $\varepsilon_{cut}{}^p$ is the cut-off strain, and n is the strain hardening exponent.

The strain rate sensitivity function is as follows:

$$\Gamma\left(\dot{\varepsilon}\right) = \left(1 + \frac{\dot{\varepsilon}}{\dot{\varepsilon}_0}\right)^{\frac{1}{m_1}} if\ \dot{\varepsilon} \le \dot{\varepsilon}_t \tag{32}$$

$$\Gamma\left(\dot{\varepsilon}\right) = \left(1 + \frac{\dot{\varepsilon}}{\dot{\varepsilon}_0}\right)^{\frac{1}{m_2}} \left(1 + \frac{\dot{\varepsilon}_t}{\dot{\varepsilon}_0}\right)^{\left(\frac{1}{m_1} - \frac{1}{m_2}\right)} \text{ if } \dot{\varepsilon} > \dot{\varepsilon}_t \tag{33}$$

where έ is the strain rate, $\acute{\varepsilon}_0$ is the reference plastic strain rate, $\acute{\varepsilon}_t$ is the strain rate of the transition between the high and low strain sensitivity, and m_1 and m_2 are the low and high strain rate sensitivity indices, respectively.

The thermal softening function is as follows:

$$\Theta(T) = c_0 + c_1 T + c_2 T^2 + c_3 T^3 + c_4 T^4 + c_5 T^5, \text{ if } T < T_{cut} \tag{34}$$

$$\Theta(T) = \Theta(T_{cut})\left(1 - \frac{T - T_{cut}}{T_{melt} - T_{cut}}\right), \text{ if } T \ge T_{cut} \tag{35}$$

where c_0–c_5 are the coefficients of the polynomial fit, T is the temperature, Tm is the melting temperature, and T_{cut} is the linear cut-off temperature.

The damage model is

$$D = \sum_i \frac{\Delta \varepsilon_i^p}{\varepsilon_{fi}^p} \tag{36}$$

where D is the dimensionless cumulative damage, $\Delta\varepsilon_i{}^p$ is the instantaneous increment of strain, and $\varepsilon^p{}_{fi}$ is the instantaneous strain to failure.

After considering the existing models, it is necessary to emphasize that the effectiveness of a model should describe material behavior by incorporating the historical effects of temperature, strain rates, load paths, and other phenomena in addition to real-time effects of temperature and strain. Until a model such as this is developed, engineers will continue to choose from the pool of existing models that suit the material being analyzed and the deformation process that the workpiece material is being subjected to. For the analysis of chip formation and associated machining phenomena when turning hub flanges, a Lagrangian-Eulerian formulated finite element model that is thermo-mechanically coupled with the power law material model was used that adaptively re-meshed itself during numerous iterative computations. Finite spatial resolutions allowed the authors to include variable cutting edge radii, primary and secondary shear zones, and chip loading phenomena that replicated industrial conditions of machining hub flanges.

3 Axle hub turning: current practice

The current practice to reduce or eliminate the crowding of chips around the tool and workpiece is associated with eliminating the generation of long, unbroken snarls of metal that is normally caused by low feeds and low/shallow depths of cut when internally boring in the longitudinal direction or internally turning to a specific profile, which is common when turning axle hub housings. Other factors include too large nose radius of the tool, or an unsuitable lead angle. The solution to avoiding chip crowding can be found by increasing the feed, selecting the geometry of the tool with better chip breaking capabilities, using high pressure coolant, selecting a smaller nose radius tool held in a holder with a large lead angle, or by varying the spindle speed.

When internally boring axle hub housings, the choice of tool is restricted to the size of the hole to be bored and the depth of the hole with the accompanying overhang. It is best to select the tool with the lowest overhang and the largest tool size to minimize deflection and vibration [1]. For roughing and light roughing cuts, it is advisable to use a negatively shaped insert with stable damping, operating the range of feeds between 0.1 and 1.5 mm/rev, while the depths of cut range between 0.1 and 10 mm. A small nose radius and angle is always preferred in order to minimize cutting forces, and the lead angle is close to 0° whenever possible. For optimizing the boring operation, a tool holder should have a square insert with a small lead angle, a rhombic-shaped insert, or a trigon-shaped insert is used for versatility with a − 5° lead angle, or a tool holder with a 55° rhombic-shaped insert with a − 3° lead angle is preferred for multi-purpose boring operations such as profiling and longitudinal boring. In order to understand the effect of changing the tool nose radius on chip formation on longitudinal boring of a small axle hub, a finite element analysis was conducted using Third Wave Systems' AdvantEdge™ software on a hub component that was manufactured from UNS G10530 steel having a chemical composition comprising the following: 0.48–0.55% carbon (C), 0.7–1% manganese (Mn), and the balance of iron (Fe). An example of the axle hub housing machined is shown in Fig. 2, which is held in a chuck of a manual center lathe manufactured by Myford of Nottingham, UK. The cross slide holds a four-way tool post carrying a boring bar complete with TiN-coated insert. A closer view of the arrangement is shown in Fig. 3. A cut-off is also located on the cross slide but is not used in this particular operation.

The machining conditions were as follows: spindle speed, n = 200 revolutions/min; depth of cut, a_p = 0.1 mm; cutting speed, v_c = 320 m/min; feed, f_n = 0.3 mm/revolution; and tool inserts DNMG 433A (3/64ths of an inch (~ 1.2 mm) nose radius) and DNMG 431A (1/64ths of an inch (~0.4 mm) nose radius) with Al_2O_3 coating on WC substrate, 0° lead angle, and a negative shape. In addition to the parameters described,

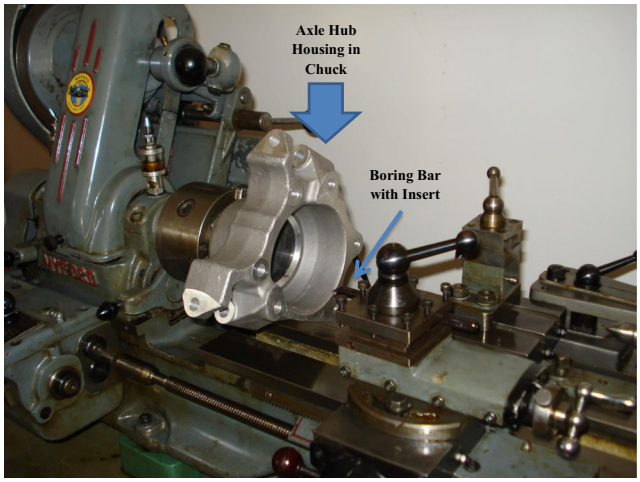

Fig. 2 Myford center lathe in preparation for longitudinal boring of the internal bearing surface of an axle hub housing. The boring bar holder and insert are shown to the right of the housing securely attached in the four-way tool holder

the standard machining equations that describe longitudinal boring are explained.

The metal removal rate for the operation is a measure of how much metal is removed per unit time and given by the following equation:

$$Q = v_c . a_p . f_n \tag{37}$$

where Q is the metal removal rate (mm^3/min), v_c is the cutting speed (mm/min), a_p is the depth of cut (mm), and f_n is the feed per revolution (mm/rev). The value of Q for the boring operation is 9600 mm^3/min. The machining time is as follows:

$$T_c = \frac{l_m}{f_n.n} \tag{38}$$

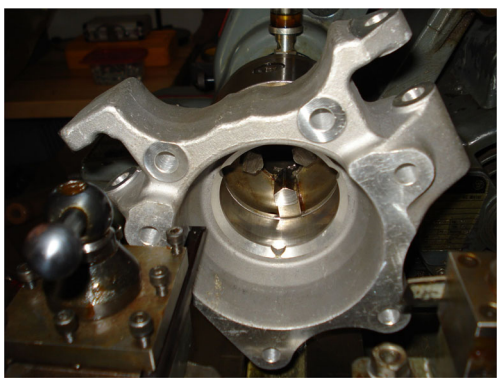

Fig. 3 Close-up view of an axle hub housing showing the position of the boring bar inside the housing

where l_m is the machined length (mm), f_n is the feed per revolution (mm/rev), and n is the spindle speed (rpm). The machining time for the boring operation is calculated as 1.67 min. The average chip thickness, h_m, is as follows:

$$h_m = f_n.\sin(90-k_r) \tag{39}$$

where f_n is the feed per revolution (mm/rev) and k_r is the lead angle (degrees). The longitudinal boring operation discussed that the average chip thickness is approximately 0.296 mm.

It is useful to compare metal cutting processes using the principles of similarity. Similarity theory is not yet fully developed for the analysis of metal cutting. However, some useful similarity numbers that can be used in modeling of the metal cutting process have been developed [15, 16].

(I) Chip compression ratio

The chip compression ratio (CCR) describes similarity of deformation in metal cutting. The energy spent on plastic deformation of a wide variety of ductile work materials is within the range of 70–80% of the total energy [17]. CCR can be used to assess the work of plastic deformation in metal cutting [17], calculate the cutting force [18], and verify the validity of a finite element model [19]. The chip compression ratio (ζ) is determined as the ratio of the length of cut (L_l) to the corresponding length of the chip (L_c) or the ratio of the chip thickness (t_2) to the uncut chip thickness (t_1), or the ratio of the cutting speed (v) to the chip velocity (v_1), i.e.,

$$\zeta = \frac{L_l}{L_c} = \frac{t_2}{t_1} = \frac{v}{v_1} \tag{40}$$

CCR is the major determining criterion of similarity in metal cutting. This is because it directly defines the elementary work spent over plastic deformation (A_u) of a unit volume of the work material as

$$A_u = 2K(\ln\zeta)^{n+1} \tag{41}$$

where K is the strength coefficient (N/m^2) and n is the hardening exponent of the work material. Figure 4 shows that the CCR is highest for the machining of copper and lowest for the machining of steel. This fact confused earlier researchers as it is well-known fact that cutting energy and forces are much greater in machining steel. Equation (41) resolves the contradiction. Referring to Fig. 4, the elementary work done is the greatest for steel. In other words, the energy per unit volume spent in the machining of steel is much greater, which results in a larger amount of heat generated and an increase in tool wear.

Therefore, a necessary condition of the similarity of two deformation processes in metal cutting is sharing an equivalent

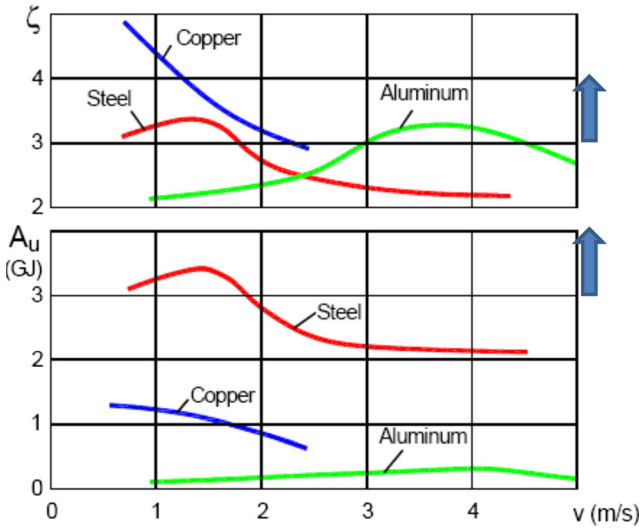

Fig. 4 The effect of cutting speed on CCR and work done in plastic deformation: (1) AISI steel 52100, (2) copper, and (3) aluminum 1050–0 [10, 11]. For G10530 axle hubs, CCR varies between 3 and 4 when machining G10530 axle hubs at a cutting speed of 320 m/min (5.33 m/s). The range for CCR is denoted by *arrows* superimposed on the figure adapted from refs. [15, 16]

value of A_u. This is of significance to the experimental studies in metal cutting because it correlates in a simple way that the work of plastic deformation done in cutting can be correlated to CCR. CCR also allows one to calculate the power spent on the plastic deformation of each layer being removed and on friction at the tool-chip interface. The power spent on the plastic deformation of the layer being removed, P_{pd}, can be calculated from the chip compression ratio and parameters of the deformation curve of the work material as follows [18],

$$P_{pd} = \frac{K(1.15\ln\zeta)^{n+1}}{n+1} vA_w \tag{42}$$

where A_w is the uncut chip cross-sectional area (m^2),

$$A_w = d_w f \tag{43}$$

where d_w is the depth of cut (m), f is the cutting feed per revolution (m/rev). CCR represents the true strain in plastic deformation and can be used to calculate the elementary work spent in plastic deformation of a unit volume of the work material. The total work done by the external force applied to the tool can then be calculated [14]. For the current longitudinal boring operation, the value of CCR is dependent on the variations in chip thickness, which vary from 0.3 to 0.4 mm. Assuming that the uncut chip thickness is 0.1 mm, CCR varies between 3 and 4 when machining G10530 axle hubs at a cutting speed of 320 m/min (5.33 m/s).

(II) Peclet number

Machining requires a moving heat source. Similarity numbers used in thermodynamics to deal with moving heat sources [20] should be utilized for thermodynamic analyses of metal cutting. This is not the case in traditional studies on thermal aspects of metal cutting. To avoid misrepresentation of the experimental data on CCR, this parameter should be determined as a function of the Peclet criterion. Such a representation allows one to account for the combined influence of the cutting regime and thermal properties of the work material. Moreover, one can assess the influence of the thermal energy generated in machining due to plastic deformation and friction on the mechanical properties of the work materials ahead of the cutting edge so that the appropriate work material model can be used in modeling (analytical, numerical, or physical). The Peclet criterion, often referred to as the Peclet number, is widely used in the thermal analysis of systems subjected to moving heat sources irrespective of temporal dimensions [20]. It is a dimensionless number expressing the ratio of advection to thermal diffusion expressed as

$$Pe = \frac{\mathbf{UL}}{w_w} \tag{44}$$

where U is the velocity scale, L is the horizontal length scale, and w_w is the thermal diffusivity. In metal cutting, the Peclet criterion is represented in terms of machining process parameters as follows,

$$Pe = \frac{vt_1}{w_w} \tag{45}$$

where v is the velocity of a moving heat source (the cutting speed) (m/s) and w_w is the thermal diffusivity of the work material (m^2/s),

$$w_w = \frac{k_w}{(c_p\rho)_w} \tag{46}$$

where k_w is the thermal conductivity of the work material, (J/(m·s·°C)), and $(c_p{\cdot}\rho)_w$ is the volume specific heat of work material, (J/($m^{3\cdot}$°C)). The Peclet number is a similarity number, which characterizes the relative influence of the cutting regime ($v.t_1$) with respect to the thermal properties of the workpiece material (w_w). If Pe > 10, then the heat source (cutting tool) moves over the workpiece faster than the velocity of thermal wave propagation in the work material so that the thermal energy generated in cutting due to the plastic deformation of the work material and due to friction at the tool-chip interface does not affect the work material ahead of the tool [16]. If Pe < 10, then the thermal energy due to plastic deformation and friction makes a strong contribution to the

process of plastic deformation during cutting, and it affects the mechanical properties of the work material when being cut. When deciding which material model to use in the finite element analysis of machining, the following should be observed to select the right model: (a) when Pe < 10, then the machining process is a hot working process, and temperature dependent machining models such as the Johnson-Cook [7], Bammann, Chiesa and Johnson [8], power law [14], and the Zerrelli and Armstrong [12] models can be used; and (b) when Pe > 10, the machining process is a cold working process where machining models can be used that do not have temperature dependence, such as the power law and mechanical threshold models.

The influence of the cutting speed on CCR for different feeds is shown in reference [15, 16]. Six complete machining tests were performed, and the results shown indicate when the Peclet criterion is used as the independent variable. Such a representation allows the reduction of the number of cutting tests needed to study the amount of plastic deformation in the metal cutting process. It reveals the mutual influence of the cutting regime, tool geometry, and physical properties of the work material on plastic deformation.

It is seen that the amount of plastic deformation in cutting for a work material having low thermal conductivity is greater compared to that in cutting a work material having high thermal conductivity. The experimental results show the correlation between the thermal conductivity of the work material and the amount of plastic deformation required to machine it, or simply a measure of 'machinability'. The tool rake angle is the only tool geometry parameter that may affect the work of plastic deformation. CCR does not depend on the tool rake angle if the Pe-criterion is used as an independent variable in machining experiments.

For the current longitudinal boring operation, the Peclet number (Pe) is calculated by knowing the cutting speed (5.33 m/s), the uncut chip thickness (0.1×10^{-3} m), and the thermal diffusivity of the material ($\sim 1.4 \times 10^{-5}$ m^2/s). Therefore, Pe is calculated to be 38 for the longitudinal boring of G10530 axle hubs.

(III) Poletica number

The tool–chip contact length, also known as the length of the tool–chip interface, determines major tribological conditions at the interface such as temperatures, stresses, tool wear, etc. Moreover, all the energy required by the system for chip removal is determined by this interface. Therefore, it is of great interest to find a way to calculate its length. To deal with the problem, the Poletica criterion (Po-criterion) is introduced [21] as the ratio of the contact length, l_c to the uncut chip thickness, t_1.

$$Po = \frac{l_c}{t_1} \tag{47}$$

The Po-criterion defines the similarity of the tribological conditions at the tool-chip interface. The major factors that affect the tool-chip contact length are the uncut chip thickness, cutting speed, and rake angle. Only the uncut chip thickness affects the contact length directly. The Pe-criterion strongly depends on CCR and weakly depends on the rake angle. The influence of rake angle is within the normal experimental scatter. Moreover, it was found that the Po-criterion remains invariant to changes in the mechanical and physical properties of the work material. The hardness of the work material does not affect the dependence of Po-criterion on CCR. Considering this experiment, one should note that beryllium copper is an excellent test material because its mechanical properties can be changed in a wide range by heat treatment while the phase composition and microstructural parameters remain practically unchanged. Relatively little scatter is reported in terms of rake angle effects, the greatest variation being in the type of work material used [14].

The normalized chip compression ratio, ζ_t, is used instead of ζ,

$$\zeta_t = \frac{\zeta}{d_{w1} \Big/ d_w} \tag{48}$$

where d_{w1} is the width of the chip. When cutting copper and pure iron, the chip width changes considerably compared to the width of cut (depth of cut). For many workpiece materials, the ratio $d_{w1}/d_w \approx 1$.

For the current longitudinal boring operation, the Poletica number (Po) is calculated by knowing the contact length (h $(2.05\xi\text{-}0.55) = 0.56$ for CCR equal to 3, or 0.765 for CCR equal to 4 and the uncut chip thickness (0.1×10^{-3} m). Therefore, Po is calculated to vary between 5.6 and 7.65 (as a function of ξ) for the longitudinal boring of G10530 axle hubs.

In summary, for the current longitudinal boring of G10530 axles hubs using the machining conditions stated, (CCR) $\xi = 3$–4, Pe = 38, and Po = 5.6–7.65. In order to characterize the predicted shape and size of machined chips and the resultant workpiece reactions to the current machining practice, a two-dimensional analysis of the machining operation was simulated by varying the radius of the edge of the insert to reduce the size of the chips and the magnitude of radial and tangential forces. The purposes of conducting the analysis are to show how chip formation takes place, how the workpiece reacts to changing the nose radius of the tool insert, and to provide possible solutions to eliminate long chip formations.

3.1 Finite element simulation (large edge radius, $f_{edge}/t_r = 0.25$)

The initial computational analysis focused on the effect of reducing the nose radius of the tool insert and

maintaining the current machining parameters that have been optimized for the machining of G10530 steel using a constant spindle and cutting speed. For the purposes of the analysis, it is necessary to characterize the effect of tool nose radius (t_r) in relation to the feed per tool edge (f_{edge}). This is easily calculated using the equation, f_{edge}/t_r. For the conditions stated here (large edge radius = 1.2 mm), f_{edge}/t_r = 0.3 mm/1.2 mm = 0.25. Figure 5 shows the results of the computational analysis. The analysis shows the action of cutting (F_C) and thrust forces (F_T) during the first few milliseconds of the cut. The transition from $F_C/F_T < 1$ (burr formation) to $F_C/F_T > 1$ (chip formation) defines the transition from burr-to-chip formation, when $F_C = F_T$. As chip formation continues, there is a subsequent increase in the magnitude of power required to form the chip. The computed temperature also increases owing to the transition from tribological sliding to the generation of heat at the primary shear zone. Figure 6 shows computed outputs of temperature, plastic strain, von Mises stress, pressure, and maximum shear stress for (f_{edge}/t_r = 0.25, (CCR) ξ = 3–4, Pe = 38, and Po = 5.6–7.65 (machining conditions: Q = 9600 mm^3/min, n = 200 revolutions/min, a_p = 0.1 mm, v_c = 320 m/min, and f_n = 0.3 mm/revolution).

Figure 6 shows the generation of long chips that do not fragment into smaller chips that can easily wrap around the cutting tool holder, become lodged inside the component, and could easily wrap itself around the component itself.

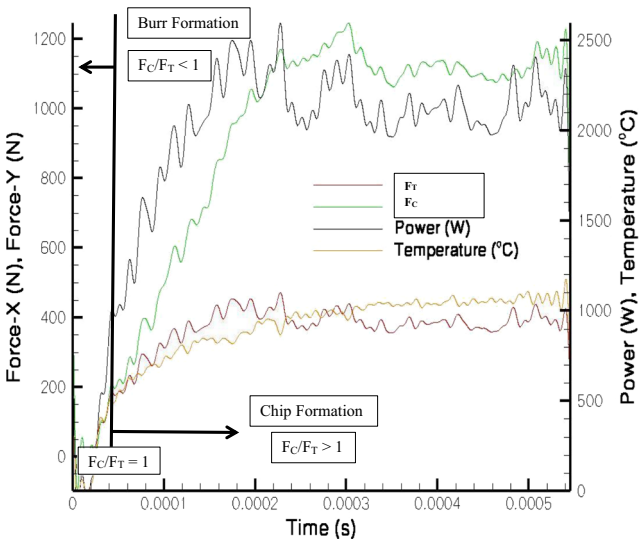

Fig. 5 Cutting and thrust force profiles for f_{edge}/t_r = 0.25 predicted by the FE method. The machining characteristics are as follows: (CCR) ξ = 3–4, Pe = 38, and Po = 5.6–7.65 (machining conditions: Q = 9600 mm^3/min, n = 200 revolutions/min, a_p = 0.1 mm, v_c = 320 m/min, and f_n = 0.3 mm/revolution). The figure shows the transition from burr-to-chip formation and the associated magnitudes of power consumed and temperature generated during the initial cut

3.2 Finite element simulation (small edge radius, f_{edge}/t_r = 0.75)

For the conditions stated here (small edge radius = 0.4 mm), f_{edge}/t_r = 0.3 mm/0.4 mm = 0.75. Figure 7 shows the results of the computational analysis. The analysis shows the action of cutting (F_C) and thrust forces (F_T) during the first few milliseconds of the cut. The transition from $F_C/F_T < 1$ (burr formation) to $F_C/F_T > 1$ (chip formation) defines the transition from burr-to-chip formation, when $F_C = F_T$. As chip formation continues, there is a subsequent increase in the magnitude of power required to form the chip. The computed temperature also increases owing to the transition from tribological sliding to the generation of heat at the primary shear zone. Figure 8 show computed outputs of temperature, plastic strain, von Mises stress, pressure, and maximum shear stress for (f_{edge}/t_r = 0.75, (CCR) ξ = 3–4, Pe = 38, and Po = 5.6–7.65 (machining conditions: Q = 9600 mm^3/min, n = 200 revolutions/min, a_p = 0.1 mm, v_c = 320 m/min, and f_n = 0.3 mm/revolution)).

Figure 8 also shows the generation of long chips that do not fragment into smaller chips that can easily wrap around the cutting tool holder, become lodged inside the component, and could easily wrap itself around the component itself. The simulations show that under current machining conditions (current practice), long chips are produced that produce unacceptable chips that decrease productivity. In these conditions, one must resort to using chip breaker geometry tools or varying the cutting speed thereby removing the expense of using expensive tools with specially defined chip breaker geometry. In order to break up the generation of long chips, variations in spindle speed were initially modeled and their results adapted to produce short chips during the practical machining operation. The next section describes how the FE method was used to predict chip shape and how further computational analysis of machining parameters were compared with analytical, closed form solutions.

4 Axle hub turning: cutting speed variation

Chip length can be reduced by simply reducing the depth of cut and variation of the spindle speed and feed of the tool into the workpiece. Boothroyd [22], Chandiramani [23], and Sandvik [24] describe the types of chips produced when cutting at various cutting speeds, feeds, and depths of cut. In their studies, they describe the types of chips produced and their classification as a function of machining characteristics (Fig. ttag9). Figure 9 shows the type of chip shapes produced under various machining conditions, i.e., constant f_n or constant a_p. The chip shape classification diagrams have been extended by industrial companies such as Sandvik Coromant to include chip breaker geometry [24].

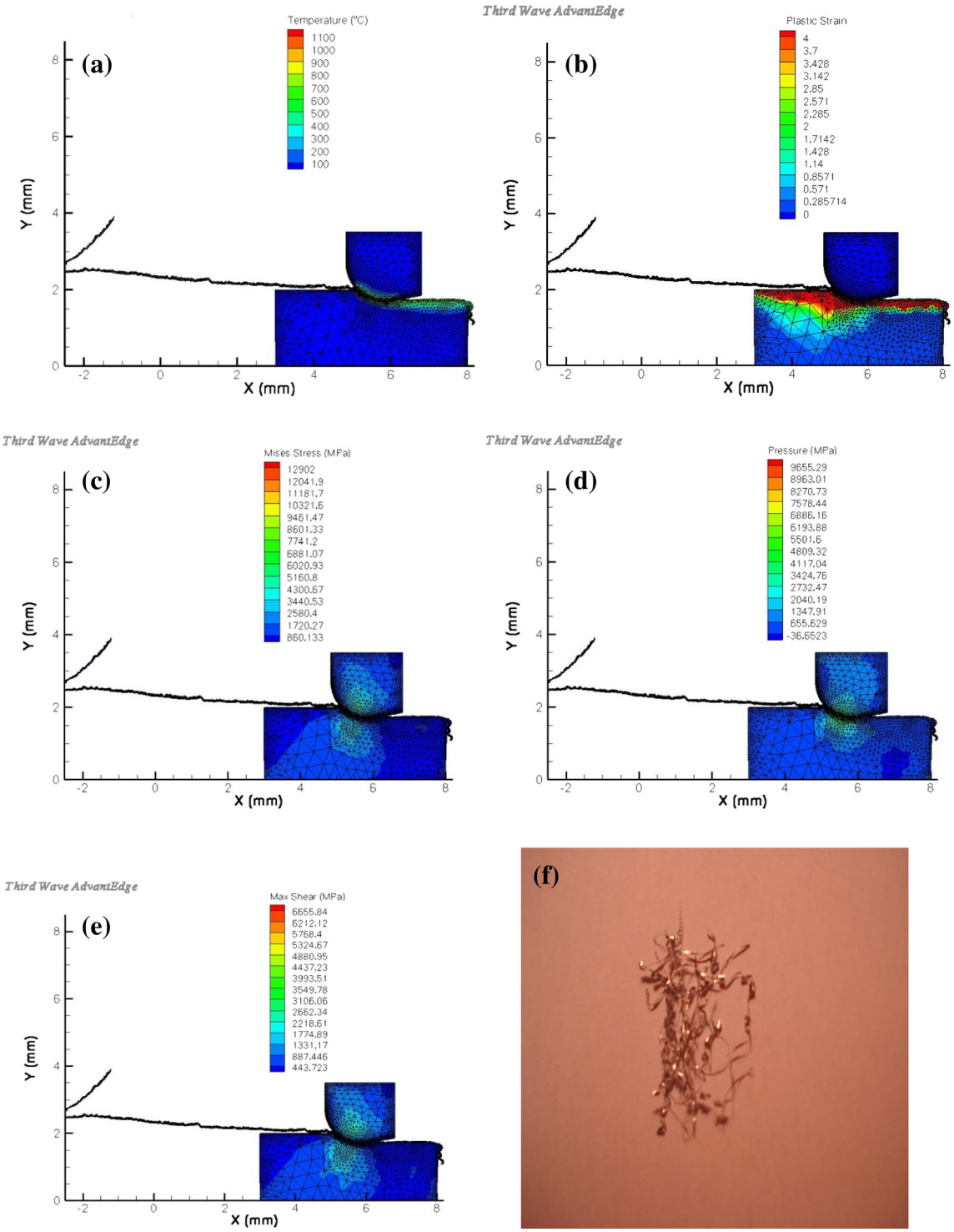

Fig. 6 Computed FE results for **a** temperature, **b** plastic strain, **c** von Mises stress, **d** pressure, and **e** maximum shear stress for the machining conditions: f_{edge}/t_r = 0.25, (CCR) ξ, = 3–4, Pe = 38, Po = 5.6–7.65, Q = 9600 mm^3/min, n = 200 revolutions/min, a_p = 0.1 mm, v_c = 320 m/min, and f_n = 0.3 mm/revolution. **f** The physical chips generated under these machining conditions

Based on the information provided by Sandvik Coromant [24] and the simulations generated based on the current practice of longitudinal boring of axle hubs, it was decided to conduct a number of computational analyses to see if the predicted chip shape can be simulated using machining conditions specified by Sandvik Coromant [24]. Three machining cases are considered: *case 1* machining conditions—v_c = 160 m/min, n = 200 rpm, a_p = 0.1 mm, f_n = 0.4 mm/rev, Q = 6400 mm^3/min; *case 2* machining conditions—v_c = 250 m/min, n = 200 rpm, a_p = 0.1 mm, f_n = 0.35 mm/

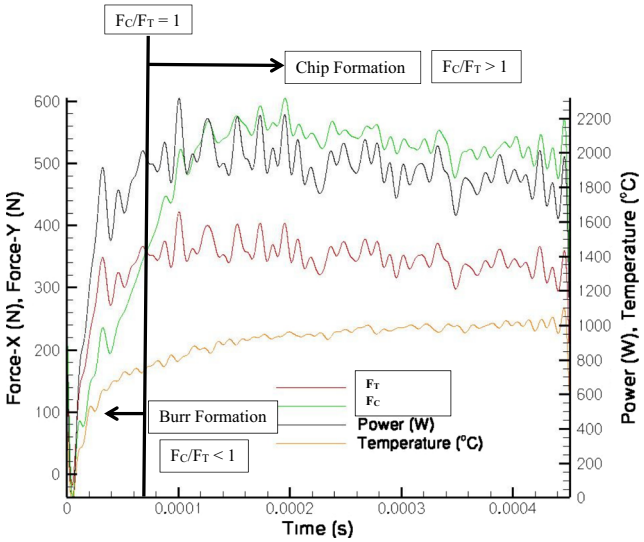

Fig. 7 Cutting and thrust force profile for $f_{edge}/t_r = 0.75$ predicted by the FE method. The machining characteristics are as follows: (CCR) $\xi = 3–4$, Pe = 38, and Po = 5.6–7.65 (machining conditions: Q = 9600 mm^3/min, n = 200 revolutions/min, a_p = 0.1 mm, v_c = 320 m/min, and f_n = 0.3 mm/revolution). The figure shows the transition from burr-to-chip formation and the associated magnitudes of power consumed and temperature generated during the initial cut

rev, Q = 8750 mm^3/min; and *case 3* machining conditions—v_c = 160 m/min, n = 200 rpm, a_p = 0.1 mm, f_n = 0.35 mm/rev, Q = 5600 mm^3/min. Cutting tool used: DNMG 431A (1/64ths of an inch (~0.4 mm) nose radius) with Al_2O_3 coating (to improve wear resistance) on a cobalt cemented tungsten carbide (WC) substrate (f_{edge}/t_r = 0.75), 0° lead angle, and a negative shape. The following case studies focus on describing the machining process for longitudinal boring of axle hub housings showing the variation caused by changes in cutting speeds and feeds.

4.1 Case 1 machining conditions—v_c = 160 m/min, n = 200 rpm, a_p = 0.1 mm, f_n = 0.4 mm/rev, Q = 6400 mm^3/min

For the conditions stated (v_c = 160 m/min, n = 200 rpm, a_p = 0.1 mm, f_n = 0.4 mm/rev, Q = 6400 mm^3/min, f_{edge}/t_r = 0.75), Fig. 10 shows the results of the computational analysis. The analysis shows the action of cutting (F_C) and thrust forces (F_T) during the first few milliseconds of the cut. The transition from burr-to-chip formation occurs when $F_C = F_T$, which is denoted by the blue arrows. Under the stated conditions, burr formation is predominant resulting in the formation of a chip when $F_C/F_T > 1$. The computed temperature increases and settles to a steady state when tribological sliding leads to the generation of heat at the primary shear zone. The figure tends to indicate that frictional sliding and the build-up of strained metal are released thus forming a chip at the points where $F_C/F_T > 1$ (these points are located immediately after the cutting force is equal to the thrust force, F_C/F_T = 1). Figure 11 shows computed outputs of temperature, plastic strain, von Mises stress, pressure, and maximum shear stress for (f_{edge}/t_r = 0.75, (CCR) $\xi = 3.5–4$, Pe = 137, and Po = 7.72–8.75 (machining conditions: Q = 6400 mm^3/min, n = 200 revolutions/min, a_p = 0.1 mm, v_c = 160 m/min, and f_n = 0.4 mm/revolution)).

4.2 Case 2 machining conditions—v_c = 250 m/min, n = 200 rpm, a_p = 0.1 mm, f_n = 0.35 mm/rev, Q = 8750 mm^3/min

For the conditions stated (v_c = 250 m/min, n = 200 rpm, a_p = 0.1 mm, f_n = 0.35 mm/rev, Q = 8750 mm^3/min, f_{edge}/t_r = 0.75), Fig. 12 shows the results of the computational analysis. The analysis shows the action of cutting (F_C) and thrust forces (F_T) during the first few milliseconds of the cut. The transition from burr-to-chip formation occurs when $F_C = F_T$, which is denoted by the blue arrows. Under the stated conditions, burr formation is predominant resulting in the formation of a chip when $F_C/F_T > 1$. The computed temperature increases and settles to a steady state when tribological sliding leads to the generation of heat at the primary shear zone. The figure tends to indicate that frictional sliding and the build-up of strained metal are released thus forming a chip at the points where $F_C/F_T > 1$ (these points are located immediately after the cutting force is equal to the thrust force, F_C/F_T = 1. Figure 13 shows computed outputs of temperature, plastic strain, von Mises stress, pressure, and maximum shear stress for (f_{edge}/t_r = 0.75, (CCR) $\xi = 3.5–4$, Pe = 157, and Po = 7.72–8.75 (mchining conditions: Q = 8750 mm^3/min, n = 200 revolutions/min, a_p = 0.1 mm, v_c = 250 m/min, and f_n = 0.35 mm/revolution)).

4.3 Case 3 machining conditions—v_c = 160 m/min, n = 200 rpm, a_p = 0.1 mm, f_n = 0.35 mm/rev, Q = 5600 mm^3/min

For the conditions stated (v_c = 160 m/min, n = 200 rpm, a_p = 0.1 mm, f_n = 0.35 mm/rev, Q = 5600 mm^3/min, f_{edge}/t_r = 0.75), Fig. 14 shows the results of the computational analysis. The analysis shows the action of cutting (F_C) and thrust forces (F_T) during the first few milliseconds of the cut. The transition from burr-to-chip formation occurs when $F_C = F_T$, which is denoted by the blue arrows. Under the stated conditions, burr formation is predominant resulting in the formation of a chip when $F_C/F_T > 1$. The computed temperature increases and settles to a steady state when tribological sliding leads to the generation of heat at the primary shear zone. The figure tends to indicate that frictional sliding and the build-up of strained metal are released thus forming a chip at the points where $F_C/F_T > 1$ (these points are located immediately after the cutting force is equal to the thrust force, F_C/F_T = 1). Figure 15 shows computed outputs of temperature, plastic strain, von Mises stress, pressure, and maximum shear stress

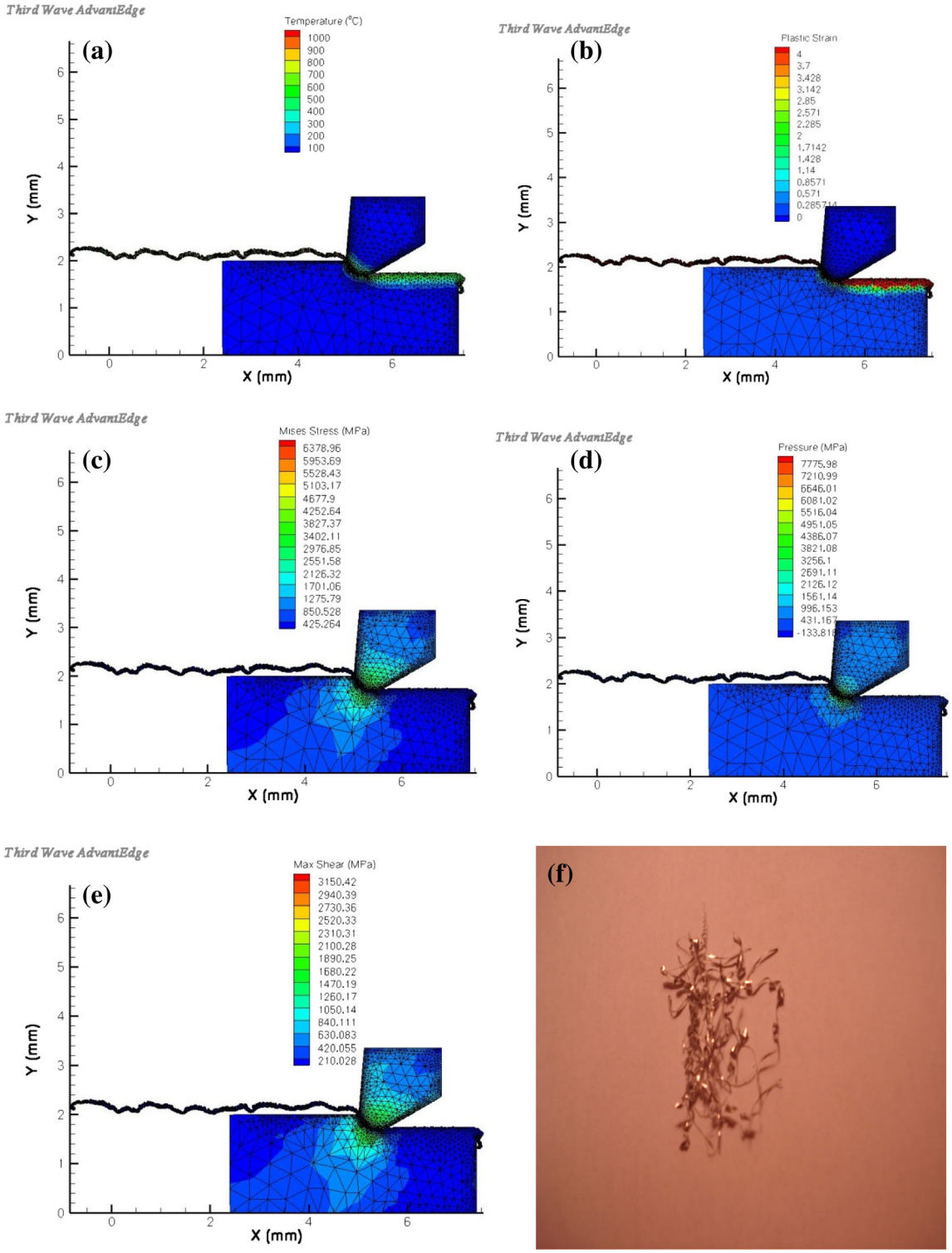

Fig. 8 Computed FE results for **a** temperature, **b** plastic strain, **c** von Mises stress, **d** pressure, and **e** maximum shear stress for the machining conditions: f_{edge}/t_r = 0.75, (CCR) ξ = 3–4, Pe = 38, Po = 5.6–7.65, Q = 9600 mm^3/min, n = 200 revolutions/min, a_p = 0.1 mm, v_c = 320 m/min, and f_n = 0.3 mm/revolution **f** The physical chips generated under these machining conditions

for (f_{edge}/t_r = 0.75, (CCR) ξ = 3.5–4, Pe = 137, and Po = 7.72–8.75 (machining conditions: Q = 5600 mm^3/min, n = 200 revolutions/min, a_p = 0.1 mm, v_c = 160 m/min, and f_n = 0.35 mm/revolution)).

In practice, and as predicted by the finite element model, the variation in cutting speed produces small broken chips that avoids the occurrence of chip crowding the tool, tool holder, and workpiece, so that chips can be flushed away using high

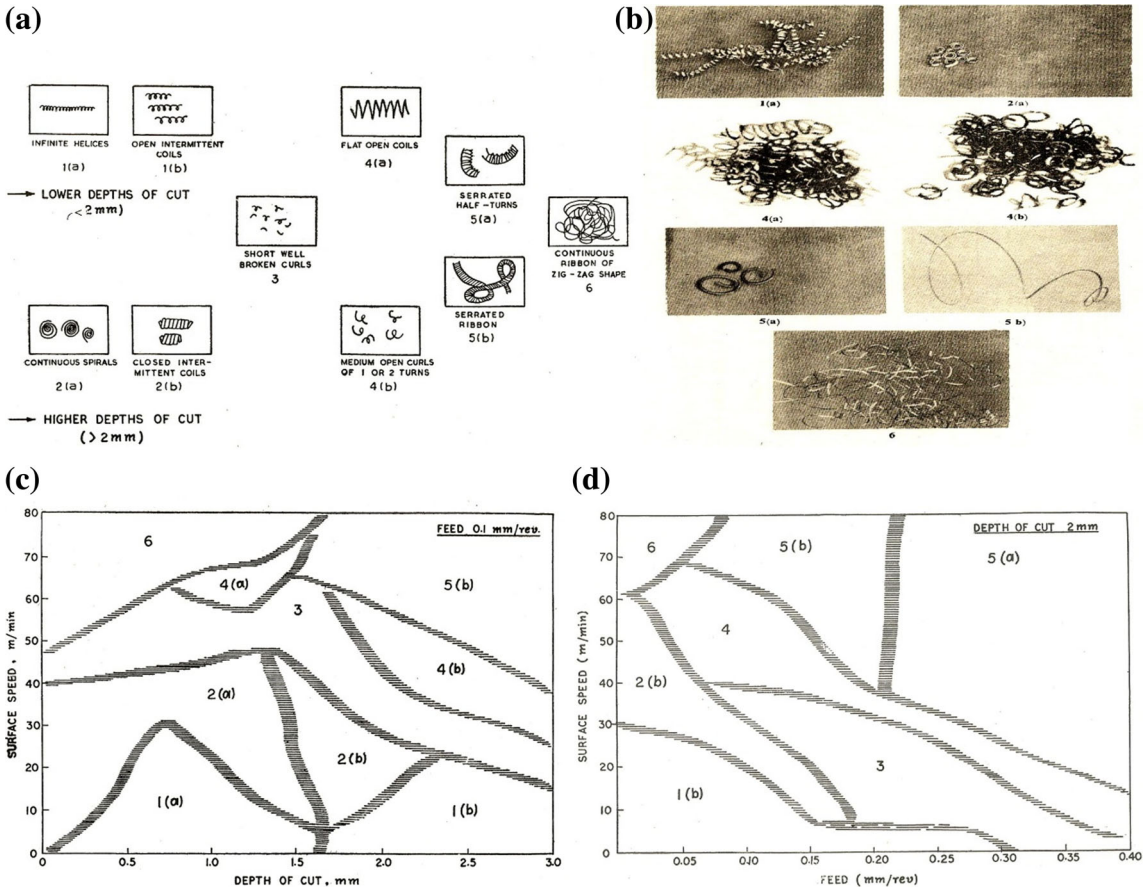

Fig. 9 Chip shape classification according to references [22, 23]. **a** Chip shape classification as a function of a_p. **b** Machined chip shapes with classifications shown in **a**, notably 1a, 2a, 4a, 4b, 5a, 5b, and 6. **c** Chip classification diagram (constant f_n). **d** Chip classification diagram (constant a_p)

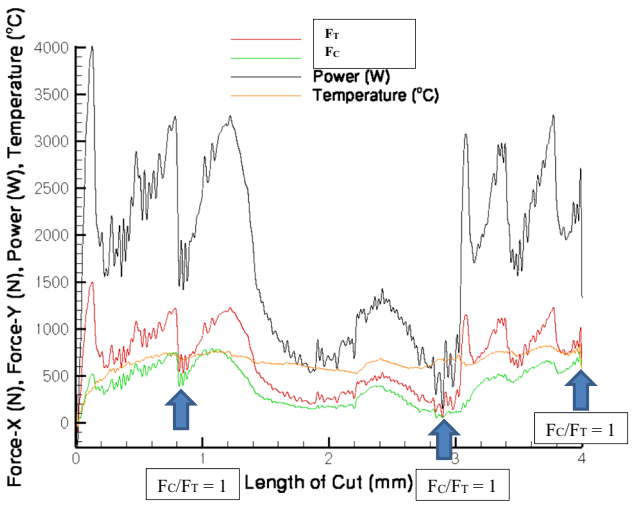

Fig. 10 Cutting and thrust force profile for $f_{edge}/t_r = 0.75$ predicted by the FE method. The machining characteristics are as follows: (CCR) $\xi = 3.5–4$, Pe = 137, and Po = 7.72–8.75 (machining conditions: Q = 6400 mm^3/min, n = 200 revolutions/min, a_p = 0.1 mm, v_c = 160 m/min, and f_n = 0.4 mm/revolution). The figure shows the transition from burr-to-chip formation ($F_C/F_T = 1$ (denoted by *blue arrows*)) and the associated magnitudes of power consumed and temperature generated during the initial cut

pressure coolant streams. This applies to the conditions simulated in case studies 1, 2, and 3. The FE method accurately predicted chip shape for each spindle speed, which was confirmed by industrial practice and chips collected, photographed, and presented in Figs. 6, 8, 11, 13, and 15. Comparisons between FE predicted machining parameters and analytical, closed form solutions are discussed in the next section of the paper.

5 Discussion

5.1 Axle hub turning: current practice ($f_{edge}/t_r = 0.25$)

For the current axle hub turning operation, the specific cutting pressure (energy consumed per unit volume of material

Fig. 11 Computed FE results for **a** temperature, **b** plastic strain, **c** ▶ maximum shear stress, **d** von Mises stress, and **e** pressure. Machining conditions: $f_{edge}/t_r = 0.75$, (CCR) $\xi = 3.5–4$, Pe = 137, Po = 7.72–8.75, Q = 6400 mm^3/min, n = 200 revolutions/min, a_p = 0.1 mm, v_c = 160 m/min, and f_n = 0.4 mm/revolution. **f** The physical chips generated under these machining conditions

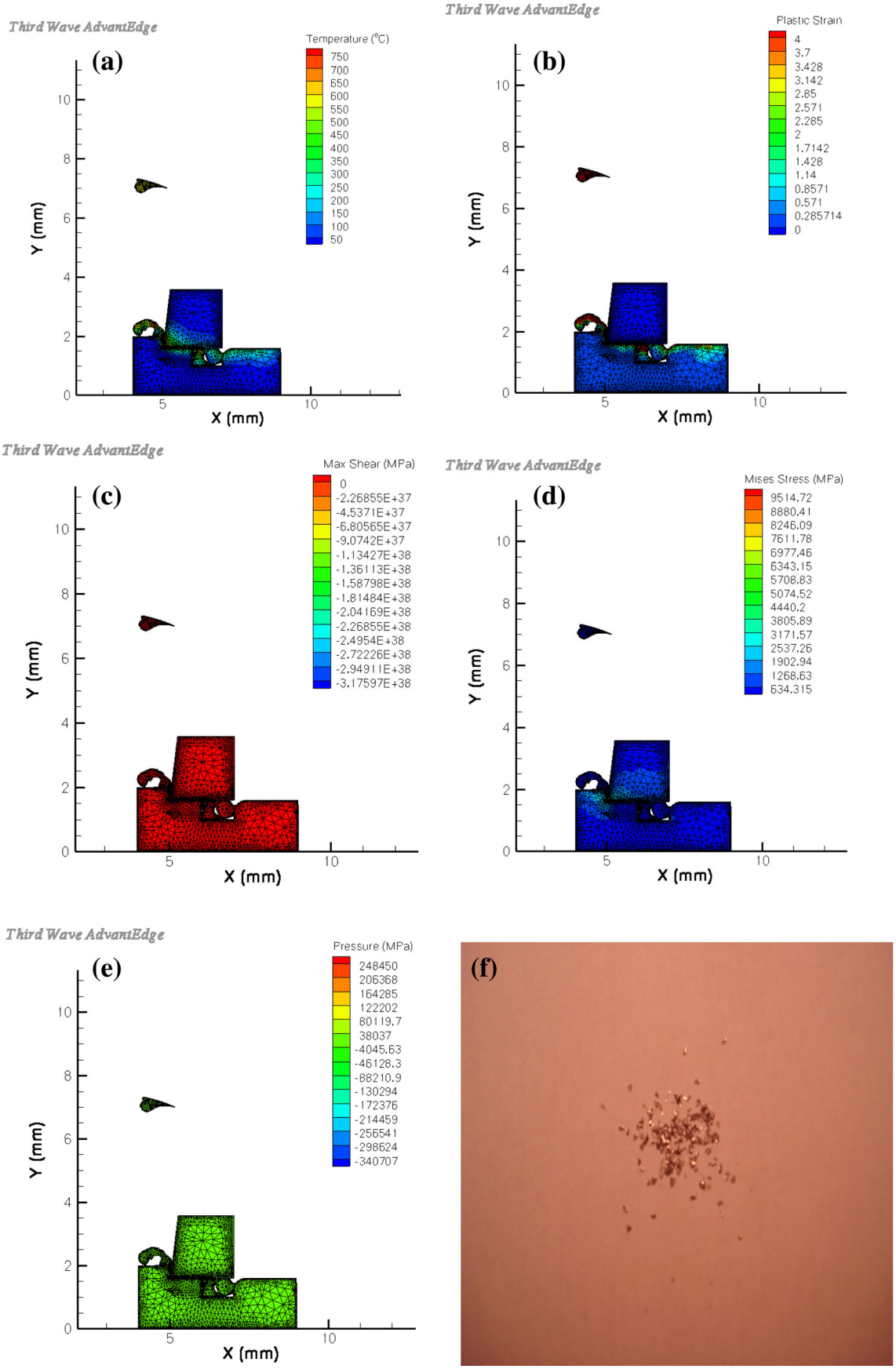
Third Wave AdvantEdge
(a)
Temperature (°C)
750
700
650
600
550
500
450
400
350
300
250
200
150
100
50
Y (mm)
X (mm)
Third Wave AdvantEdge
(b)
Plastic Strain
4
3.7
3.428
3.142
2.85
2.571
2.285
2
1.7142
1.428
1.14
0.8571
0.571
0.285714
0
Y (mm)
X (mm)
Third Wave AdvantEdge
(c)
Max Shear (MPa)
0
-2.26855E+37
-4.5371E+37
-6.80565E+37
-9.0742E+37
-1.13427E+38
-1.36113E+38
-1.58798E+38
-1.81484E+38
-2.04169E+38
-2.26855E+38
-2.4954E+38
-2.72226E+38
-2.94911E+38
-3.17597E+38
Y (mm)
X (mm)
Third Wave AdvantEdge
(d)
Mises Stress (MPa)
9514.72
8880.41
8246.09
7611.78
6977.46
6343.15
5708.83
5074.52
4440.2
3805.89
3171.57
2537.26
1902.94
1268.63
634.315
Y (mm)
X (mm)
Third Wave AdvantEdge
(e)
Pressure (MPa)
248450
206368
164285
122202
80119.7
38037
-4045.63
-46128.3
-88210.9
-130294
-172376
-214459
-256541
-298624
-340707
Y (mm)
X (mm)
(f)

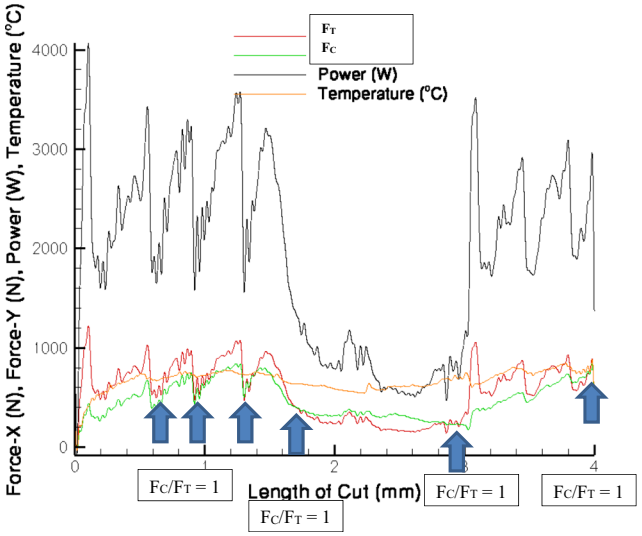

Fig. 12 Cutting and thrust force profile for $f_{edge}/t_r = 0.75$ predicted by the FE method. The machining characteristics are as follows: (CCR) $\xi = 3.5–4$, Pe = 157, and Po = 7.72–8.75 (machining conditions: Q = 8750 mm^3/min, n = 200 revolutions/min, a_p = 0.1 mm, v_c = 250 m/min, and f_n = 0.35 mm/revolution). The figure shows the transition from burr-to-chip formation ($F_C/F_T = 1$ (denoted by *blue arrows*)) and the associated magnitudes of power consumed and temperature generated during the initial cut

removed) is given by the following equation: $p_s = F_C/A_O$, where F_C is the cutting force and A_O is the area of cut. When $f_{edge}/t_r = 0.25$, (CCR) $\xi = 3–4$, Pe = 38, and Po = 5.6–7.65 (machining conditions: Q = 9600 mm^3/min, n = 200 revolutions/min, a_p = 0.1 mm, v_c = 320 m/min and f_n = 0.3 mm/revolution), the magnitude of force for the onset of burr formation is $F_C \sim 200$ N (Fig. 5), and for chip formation, it is $F_C \sim 1200$ N (Fig. 5). The area of cut, A_O, is equal to the depth of cut multiplied by the length of cut, or A_O = 0.1 mm × 0.1 mm = 0.01 mm^2. When $f_{edge}/t_r = 0.25$, specific pressure for burr formation is $p_s \sim 20$ kN/mm^2, and for chip formation, it is $p_s \sim 120$ kN/mm^2.

The rate of energy consumption (heating rate) is given by the following equation: $W_C = F_C.v_C$, where v_C is the cutting speed. When $f_{edge}/t_r = 0.25$, the heating rate for burr formation is W_C = 200 N × 320 m/min × 1/60 s/min = 1067 Nm/s (or 1067 W). For chip formation, W_C = 1200 N × 320 m/min × 1/60 s/min = 6400 Nm/s (or 6400 W).

For chip formation conditions, when $f_{edge}/t_r = 0.25$, (i) the rate of heat generated by friction between chip and cutting tool is given by the following equation: $P_f = F_f.\ v_C.\ r_C$, where r_C is the chip thickness ratio and F_f is the friction force. For boring, $F_f = F_C$ because the working normal rake angle, γ_{ne}, is zero. CCR is the chip thickness divided by the uncut chip thickness, i.e., CCR = 0.296 mm/0.1 mm = 2.96. The chip thickness ratio is given by the following equation: r_C = 0.1 mm/0.296 mm = 0.34. Therefore, the rate of heat generated by friction between chip and cutting tool, P_f = 1200 N × 320 m/min × 1/60 s/min × 0.34 = 2176 J/s; (ii) the rate of heat generation from shearing, $P_s = P_m - P_f$, or $P_s = (F_C.v_C) - P_f$. Thus, P_s = (1200 N × 320 m/min × 1/60 s/min)—2176 J/s = 4224 J/s; (iii) the temperature rise in shearing, θ_s, is first calculated using the equation, $\theta_s = ((1-\beta).P_s)/\rho.c.v_{ac}.a_w$. However, to find β, we need to find $R_T.\tan\varphi$ using Boothroyd's relationship for β as a function of $R_T.\tan\varphi$ [25].

To calculate thermal number (R_T), we must know the density (ρ), thermal conductivity (k), and specific heat capacity (c) of G10530 steel. According to various property databases, ρ = 7700 kg/m^3, k = 54 J/smK, and c = 510 J/kgK. Therefore, R_T = (7700 kg/m^3 × 510 J/kgK × 320 m/min × 1/60 s/min × 0.1 × 10^{-3} m)/54 J/smK = 38.78. Owing to the fact that the working normal rake angle, γ_{ne}, is zero, $\tan\varphi = r_C$. Thus, $R_T.\tan\varphi$ = 38.78 × 0.34 = 13.18. From Fig. 16, the value of β when $R_T.\tan\varphi$ = 13.18 is ~0.09. Now, $\theta_s = ((1-\beta).P_s)/\rho.c.v_{ac}.a_w$, where a_w is the width of cut = 10 mm (10 × 10^{-3} m). Therefore, θ_s = ((1–0.09) × 4224 J/s)/(7700 kg/m^3 × 510 J/kgK × 320 m/min × 1/60 s/min × 0.1 × 10^{-3} m × 10 × 10^{-3} m) = 183.53 °C, which is the mean temperature rise in the primary shear zone. The mean temperature rise in the secondary shear zone (frictional heating), $\theta_f = P_f/\rho.c.v_{ac}.a_w$ = (2176 J/s)/7700 kg/m^3 × 510 J/kgK × 320 m/min × 1/60 s/min × 0.1 × 10^{-3} m × 10 × 10^{-3} m) = 103.9 °C. The width of the secondary deformation zone divided by the chip thickness for unlubricated steel is γ = 0.2. The dimensionless length of the contact between chip and cutting tool (α_1) is stated by Boothroyd [25] to be the chip contact length (l_f) multiplied by the cutting ratio (r_C) divided by the chip thickness (a_o), i.e., $\alpha_1 = (l_f.r_C)/a_o$. For the present case, α_1 = (0.5 mm × 0.34)/0.296 mm = 0.574. Therefore, R_T/α_1 = 38.78/0.574 = 67.56. From Fig. 17, the value of θ_m/θ_f for the case where γ = 0.2 is ~4.2. Hence, θ_m = 4.2 × 103.9 °C = 436.4 °C. The maximum temperature, $\theta_{max} = \theta_m + \theta_f + \theta_o$ = 436.4 + 103.9 + 22 = 562.3 °C, where θ_o is the room temperature.

According to Fig. 6 and at the start of cutting, the maximum temperature is computed to be ~600 °C, which is very close to the calculated value of 562.3 °C. The types of chips produced are long and stringy and they are of the type, which are detrimental to the efficient operation of the boring process. The physical images of chips produced shown in Fig. 6 compare well with those predicted using the FE method.

For burr formation conditions when $f_{edge}/t_r = 0.25$ and for frictional heating conditions, the heat generated, $P_f = F_f.\ v_C.\ r_C$, where r_C is the chip thickness ratio and F_f is the friction

Fig. 13 Computed FE results for **a** temperature, **b** plastic strain, **c** maximum shear stress, **d** von Mises stress, and **e** pressure. Machining conditions: $f_{edge}/t_r = 0.75$, (CCR) $\xi = 3.5–4$, Pe = 137, Po = 7.72–8.75, Q = 8750 mm^3/min, n = 200 revolutions/min, a_p = 0.1 mm, v_c = 250 m/min, and f_n = 0.35 mm/revolution. **f** The physical chips generated under these machining conditions

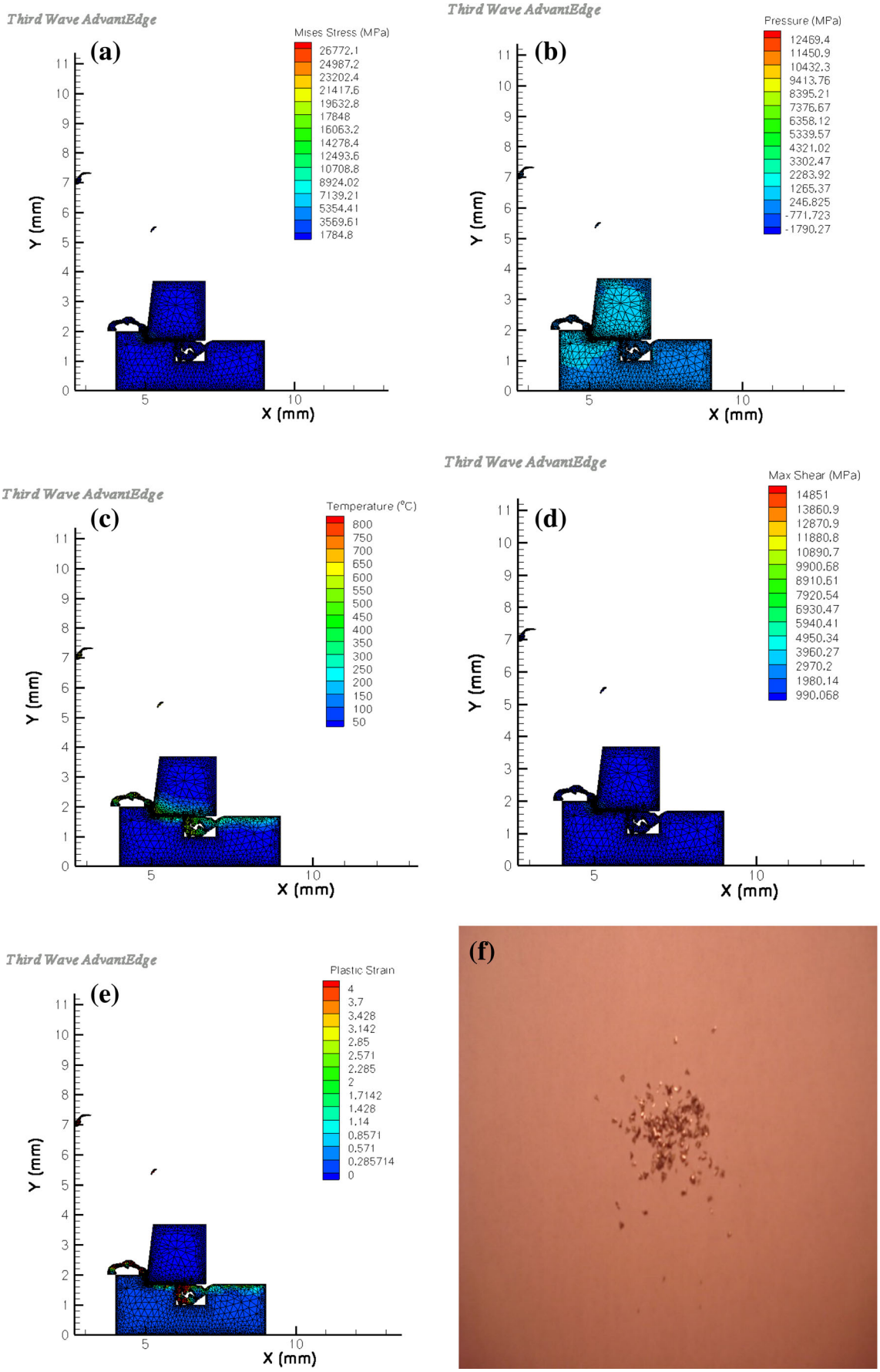
Third Wave AdvantEdge
(a)
Mises Stress (MPa)
26772.1
24987.2
23202.4
21417.6
19632.8
17848
16063.2
14278.4
12493.6
10708.8
8924.02
7139.21
5354.41
3569.61
1784.8
Y (mm)
X (mm)
Third Wave AdvantEdge
(b)
Pressure (MPa)
12469.4
11450.9
10432.3
9413.76
8395.21
7376.67
6358.12
5339.57
4321.02
3302.47
2283.92
1265.37
246.825
-771.723
-1790.27
Y (mm)
X (mm)
Third Wave AdvantEdge
(c)
Temperature (°C)
800
750
700
650
600
550
500
450
400
350
300
250
200
150
100
50
Y (mm)
X (mm)
Third Wave AdvantEdge
(d)
Max Shear (MPa)
14851
13860.9
12870.9
11880.8
10890.7
9900.68
8910.61
7920.54
6930.47
5940.41
4950.34
3960.27
2970.2
1980.14
990.068
Y (mm)
X (mm)
Third Wave AdvantEdge
(e)
Plastic Strain
4
3.7
3.428
3.142
2.85
2.571
2.285
2
1.7142
1.428
1.14
0.8571
0.571
0.285714
0
Y (mm)
X (mm)
(f)

force. When no chip is being cut, CCR = 0 and $r_C = 1$. Therefore, P_f = 200 N × 320 m/min × 1/60 s/min × 1 = 1066.67 J/s. For shearing, no heat is generated because no chip is forming. Under these conditions, the equations related to the tribology of rubbing bodies are applicable.

5.2 Axle hub turning: current practice ($f_{edge}/t_r = 0.75$)

When $f_{edge}/t_r = 0.75$, CCR (ξ) is equal to 3 to 4, Pe = 38, and Po = 5.6–7.65 (for machining conditions: Q = 9600 mm^3/min, n = 200 revolutions/min, a_p = 0.1 mm, v_c = 320 m/min, and f_n = 0.3 mm/revolution). The magnitude of force for the onset of burr formation is $F_C \sim 350$ N (Fig. 7), and for chip formation, it is $F_C \sim 600$ N (Fig. 7). Specific cutting pressure (energy consumed per unit volume of material removed) is given by the following equation: $p_s = F_C/A_O$, where F_C is the cutting force and A_O is the area of cut. The area of cut, A_O, is equal to the depth of cut multiplied by the length of cut, or A_O = 0.1 mm × 0.1 mm = 0.01 mm^2. When $f_{edge}/t_r = 0.75$, the specific pressure for burr formation is $p_s \sim 35$ kN/mm^2, and for chip formation, it is $p_s \sim 60$ kN/mm^2.

The rate of energy consumption (heating rate) is given by the following equation: $W_C = F_C.v_C$, where v_C is the cutting speed. When $f_{edge}/t_r = 0.75$, the heating rate for burr formation is W_C = 350 N × 320 m/min × 1/60 s/min = 1866 Nm/s (or 1866 W). For chip formation, W_C = 600 N × 320 m/min × 1/60 s/min = 3200 Nm/s (or 3200 W).

For chip formation conditions when $f_{edge}/t_r = 0.75$: (i) the rate of heat generated by friction between chip and cutting tool, $P_f = F_f.\ v_C.\ r_C$, where r_C is the chip thickness ratio and F_f is the friction force. For boring, $F_f = F_C$ because the working normal rake angle, γ_{ne}, is zero. CCR is the chip thickness divided by the uncut chip thickness, i.e., CCR = 0.296 mm/0.1 mm = 2.96. The chip thickness ratio, r_C = 0.1 mm/0.296 mm = 0.34. Therefore, P_f = 600 N × 320 m/min × 1/60 s/min × 0.34 = 1088 J/s; (ii) the rate of heat generation from shearing, $P_s = P_m - P_f$, or $P_s = (F_C.v_C) - P_f$. Thus, the rate of heat generation from shearing, P_s = (600 N × 320 m/min × 1/60 s/min)–1088 J/s = 2112 J/s; (iii) the temperature rise in shearing, θ_s, is first calculated using the equation, $\theta_s = ((1-\beta).P_s)/\rho.c.v_{ac}.a_w$. However, to find β, we need to find R_T.tan φ using Boothroyd's relationship for β as a function of R_T. tan φ [25].

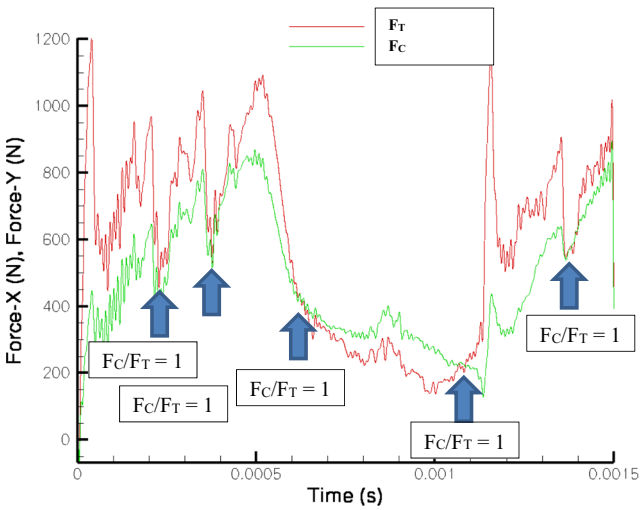

Fig. 14 Cutting and thrust force profile for $f_{edge}/t_r = 0.75$ predicted by the FE method. The machining characteristics are as follows: (CCR) ξ = 3.5–4, Pe = 137, and Po = 7.72–8.75 (machining conditions: Q = 5600 mm^3/min, n = 200 revolutions/min, a_p = 0.1 mm, v_c = 160 m/min, and f_n = 0.35 mm/revolution). The figure shows the transition from burr-to-chip formation ($F_C/F_T = 1$ (denoted by blue arrows))

To calculate thermal number (R_T), we must know the density (ρ), thermal conductivity (k), and specific heat capacity (c) of G10530 steel. According to various property databases, ρ = 7700 kg/m^3, k = 54 J/smK, and c = 510 J/kgK. Therefore, R_T = (7700 kg/m^3 × 510 J/kgK × 320 m/min × 1/60 s/min × 0.1 × 10^{-3} m)/54 J/smK = 38.78. Owing to the fact that the working normal rake angle, γ_{ne}, is zero, tan φ = r_C. Thus, R_T.tan φ = 38.78 × 0.34 = 13.18. From Fig. 16, the value of β when R_T.tan φ = 13.18 is ~0.09. Now, the temperature rise in shearing, $\theta_s = ((1-\beta).P_s)/\rho.c.v_{ac}.a_w$, where a_w is the width of cut = 10 mm (10 × 10^{-3} m). Therefore, θ_s = ((1–0.09) × 2112 J/s)/(7700 kg/m^3 × 510 J/kgK × 320 m/min × 1/60 s/min × 0.1 × 10^{-3} m × 10 × 10^{-3} m) = 91.76 °C, which is the mean temperature rise in the primary shear zone. The mean temperature rise in the secondary shear zone (frictional heat), $\theta_f = P_f/\rho.c.v_{ac}.a_w$ = (1088 J/s)/7700 kg/m^3 × 510 J/kgK × 320 m/min × 1/60 s/min × 0.1 × 10^{-3} m × 10 × 10^{-3} m) = 51.95 °C. The width of the secondary deformation zone divided by the chip thickness for unlubricated steel is γ = 0.2. The dimensionless length of the contact between chip and cutting tool (α_1) is stated by Boothroyd [25] to be the chip contact length (l_f) multiplied by the cutting ratio (r_C) divided by the chip thickness (a_o), i.e., $\alpha_1 = (l_f.r_C)/a_o$. For the present case, α_1 = (0.5 mm × 0.34)/0.296 mm = 0.574. Therefore, R_T/α_1 = 38.78/0.574 = 67.56. From Fig. 17, the value of θ_m/θ_f for γ = 0.2 is ~4.2. Hence, θ_m = 4.2 × 51.95 °C = 218.2 °C. The maximum temperature, $\theta_{max} = \theta_m + \theta_f + \theta_o$ = 218.2 + 51.95 + 22 = 292.15 °C, where θ_o is the room temperature.

The types of chips produced are long and stringy and they are of the type, which are detrimental to the efficient operation of the boring process. The physical images of chips produced shown in Fig. 8 compare well with those predicted using the FE method.

For burr formation conditions when $f_{edge}/t_r = 0.75$ and for frictional heating conditions, the heat generated, $P_f = F_f.\ v_C.\ r_C$, where r_C is the chip thickness ratio and F_f is the friction force. When no chip is being cut, CCR = 0 and $r_C = 1$. Therefore, P_f = 350 N × 320 m/min × 1/60 s/min × 1 = 1866.67 J/s. For shearing, no heat is generated because no chip is forming. Under these conditions, the equations related to the tribology of rubbing bodies are applicable. According to Fig. 8 and at the start of cutting, the maximum temperature is computed to be ~300 °C, which is very close to the calculated value of 292.15 °C.

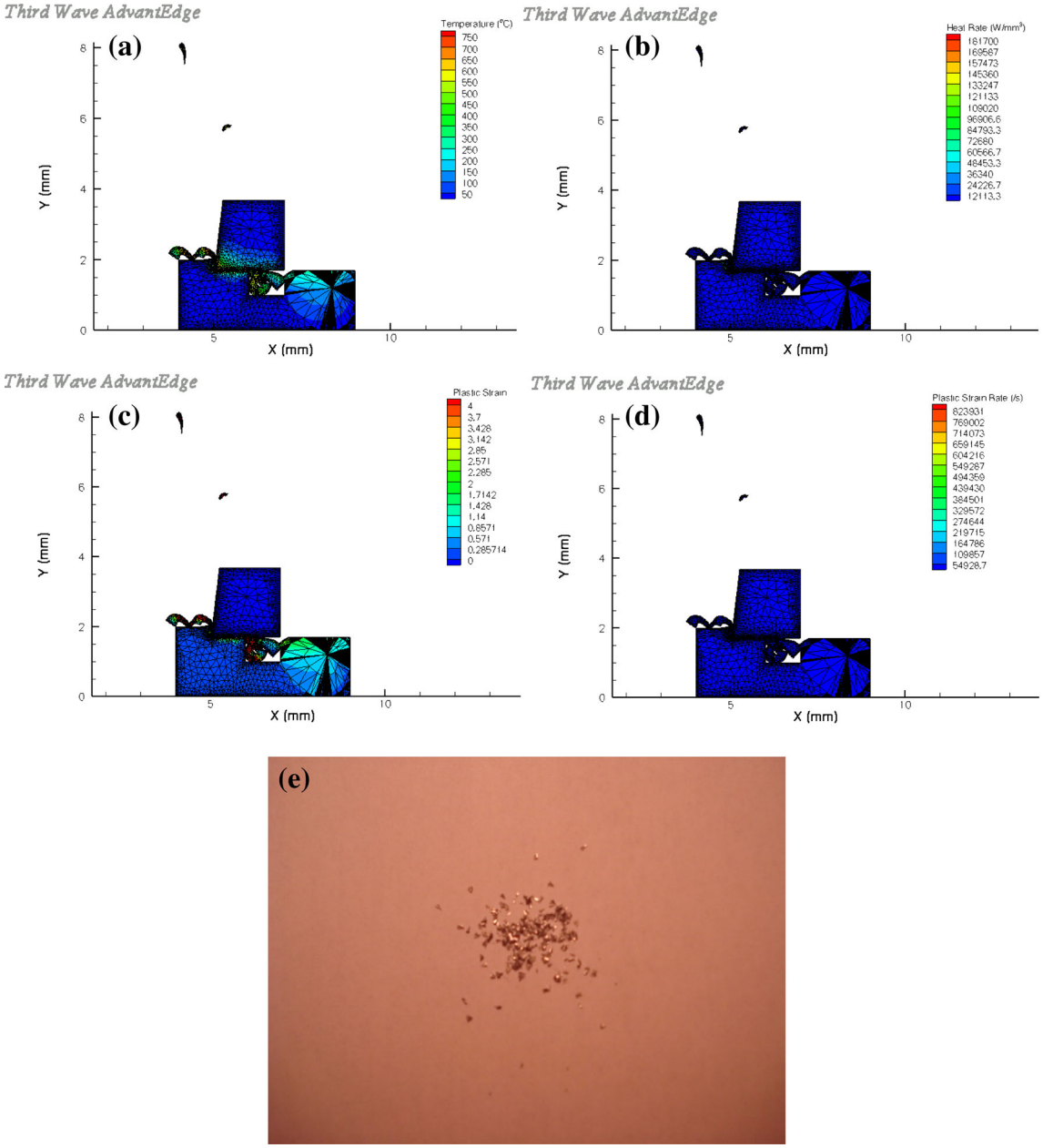

Fig. 15 Computed FE results for **a** temperature, **b** heating rate, **c** plastic strain, and **d** plastic strain rate. Machining conditions: f_{edge}/t_r = 0.75, (CCR) ξ = 3.5–4, Pe = 137, Po = 7.72–8.75, Q = 5600 mm^3/min, n = 200 revolutions/min, a_p = 0.1 mm, v_c = 160 m/min, and f_n = 0.35 mm/revolution. **e** The physical chips generated under these machining conditions

5.3 Axle hub turning: cutting speed variations (f_{edge}/t_r = 0.75)

5.3.1 Case 1 machining conditions—v_c = 160 m/min, n = 200 rpm, a_p = 0.1 mm, f_n = 0.4 mm/rev, Q = 6400 mm^3/min

The magnitude of force for the onset of chip formation varies between F_C ~ 200 N and 600 N (Fig. 9). The specific cutting pressure (energy consumed per unit volume of material removed), $p_s = F_C/A_O$, where F_C is the cutting force and A_O is the area of cut. The area of cut, A_O, is equal to the depth of cut multiplied by the length of cut, or A_O = 0.1 mm × 0.1 mm = 0.01 mm^2. When f_{edge}/t_r = 0.75, the variable specific cutting pressure, p_s, for chip formation is ~20 to 60 kN/mm^2. The rate of energy consumption (heating rate) is given by the following equation: $W_C = F_C.v_C$, where v_C is the cutting speed. When f_{edge}/t_r = 0.75, the heating rate for chip formation is W_C ~ (200 to 600) N × 160 m/min × 1/60 s/min ~ 533 W to 1600 W.

For chip formation conditions when f_{edge}/t_r = 0.75: (i) the rate of heat generated by friction between chip and cutting tool,

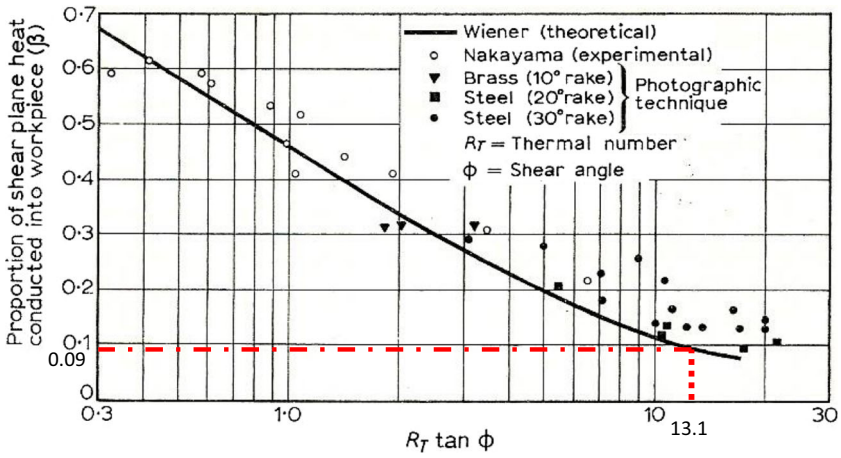

Fig. 16 Effect of R.tan φ on the division of shear zone heat between chip and workpiece material, where β is the proportion of shear zone heat conducted into the workpiece, R_T is the thermal number, and φ is the shear plane angle [25]

$P_f = F_f . v_C . r_C$, where r_C is the chip thickness ratio and F_f is the friction force. For boring, $F_f = F_C$ because the working normal rake angle, γ_{ne}, is zero. CCR is the chip thickness divided by the uncut chip thickness, i.e., CCR = 0.296 mm/0.1 mm = 2.96. The chip thickness ratio, r_C = 0.1 mm/0.296 mm = 0.34. Therefore, P_f ~ (200 to 600) N × 160 m/min × 1/60 s/min × 0.34 ~ 181 J/s to 544 J/s; (ii) the rate of heat generation from shearing, $P_s = P_m - P_f$, or $P_s = (F_C.v_C) - P_f$. Thus, P_s = ((200 to 600) N × 160 m/min × 1/60 s/min)–181 J/s or 544 J/s = 352 J/s to 1056 J/s; (iii) the temperature rise in shearing, θ_s, is first calculated using the equation, $\theta_s = ((1-\beta).P_s)/\rho.c.v_{ac}.a_w$. However, to find β, we need to find R_T.tan φ using Boothroyd's relationship for β as a function of R_T. tan φ [20].

To calculate thermal number (R_T), we must know the density (ρ), thermal conductivity (k), and specific heat capacity (c) of G10530 steel. According to various property databases, ρ = 7700 kg/m^3, k = 54 J/smK, and c = 510 J/kgK. Therefore, R_T = (7700 kg/m^3 × 510 J/kgK × 160 m/min × 1/60 s/min × 0.1 × 10^{-3} m)/54 J/smK = 19.39. Owing to the fact that the working normal rake angle, γ_{ne}, is zero, tan φ = r_C. Thus, R_T.tan φ = 19.39 × 0.34 = 6.59. From Fig. 16, the value of β when R_T.tan φ = 6.59 is ~0.16. Now, $\theta_s = ((1-\beta).P_s)/\rho.c.v_{ac}.a_w$, where a_w is the width of cut = 10 mm (10 × 10^{-3} m). Therefore, θ_s = ((1–0.16) × (352 to 1056 J/s)/(7700 kg/m^3 × 510 J/kgK × 160 m/min × 1/60 s/min × 0.1 × 10^{-3} m × 10 × 10^{-3} m) = 28.24 °C to 84.72 °C, which is the mean variable temperature rise in the primary shear zone. The mean variable temperature rise in the secondary shear zone (frictional heat) is given by the following equation: $\theta_f = P_f/\rho.c.v_{ac}.a_w$ = (181 to 544 J/s)/7700 kg/m^3 × 510 J/kgK × 160 m/min × 1/60 s/min × 0.1 × 10^{-3} m × 10 × 10^{-3} m) = 17.28 °C to 51.95 °C. The width of the secondary deformation zone divided by the chip thickness for unlubricated steel, γ = 0.2. The dimensionless length of the contact between chip and cutting tool (α_1) is stated by Boothroyd [20] to be the chip contact length (l_f) multiplied by the cutting ratio (r_C) divided by the chip thickness (a_o), i.e., $\alpha_1 = (l_f.r_C)/a_o$. For the present case, α_1 = (0.5 mm × 0.34)/0.296 mm = 0.574. Therefore, R_T/α_1 = 19.39/0.574 = 33.78. From Fig. 17, the value of θ_m/θ_f for γ = 0.2 is ~3.9. Hence, θ_m = 3.9 × (17.28 °C to 51.95)°C = 67.4 °C to 202.6 °C. The variable maximum temperature, $\theta_{max} = \theta_m + \theta_f + \theta_o$ = (67.4 to 202.6) + (17.28 to 51.95) + 22 = 106.7 °C to 276.55 °C, where θ_o is the room temperature.

According to Fig. 10 and at the start of cutting, the maximum temperature is computed to be ~300 °C, which is very close to the calculated value of 276.55 °C. The types of chips produced are short and blocky and are beneficial to the efficient operation of the boring process. The physical images of chips produced shown in Fig. 10 compare well with those predicted using the FE method.

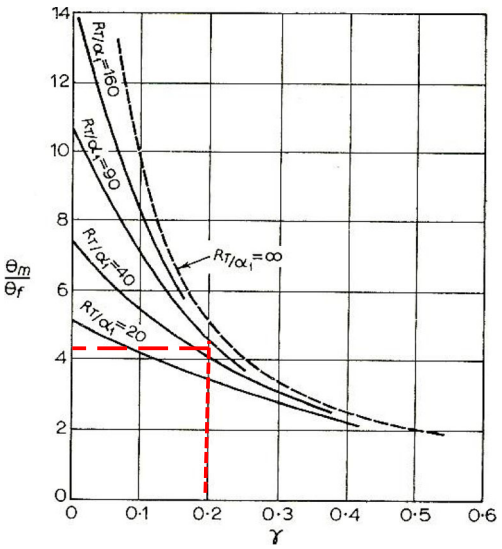

Fig. 17 Effect of width of secondary deformation zone on chip temperature, where R_T is the thermal number, α_1 is the chip-tool contact length, γ is the width of the secondary deformation zone, θ_m is the maximum temperature rise in the chip, and θ_f is the mean temperature rise in the chip [25]

5.3.2 Case 2 machining conditions—v_c = 250 m/min, n = 200 rpm, a_p = 0.1 mm, f_n = 0.35 mm/rev, Q = 8750 mm^3/min

The magnitude of force for the onset of chip formation varies between F_C ~ 200 N and 800 N (Fig. 11). The specific cutting pressure (energy consumed per unit volume of material removed), $p_s = F_C/A_O$, where F_C is the cutting force and A_O is the area of cut. The area of cut, A_O, is equal to the depth of cut multiplied by the length of cut, or A_O = 0.1 mm × 0.1 mm = 0.01 mm^2. When f_{edge}/t_r = 0.75, the variable specific cutting pressure, p_s, for chip formation is ~20 to 80 kN/mm^2.

The rate of energy consumption (heating rate) is given by the following equation: $W_C = F_C.v_C$, where v_C is the cutting speed. When f_{edge}/t_r = 0.75, the heating rate for chip formation is W_C ~ (200 to 800) N × 250 m/min × 1/60 s/min ~ 833 W to 3333 W. For chip formation conditions when f_{edge}/t_r = 0.75: (i) the rate of heat generated by friction between chip and cutting tool, $P_f = F_f.\ v_C.\ r_C$, where r_C is the chip thickness ratio and F_f is the friction force. For boring, $F_f = F_C$ because the working normal rake angle, γ_{ne}, is zero. CCR is the chip thickness divided by the uncut chip thickness, i.e., CCR = 0.296 mm/0.1 mm = 2.96. The chip thickness ratio, r_C = 0.1 mm/0.296 mm = 0.34. Therefore, P_f ~ (200 to 800) N × 250 m/min × 1/60 s/min × 0.34 ~ 283 J/s to 1133 J/s; (ii) the rate of heat generation from shearing, $P_s = P_m$-P_f, or $P_s = (F_C.v_C)$-P_f. Thus, P_s = ((200 to 800) N × 250 m/min × 1/60 s/min)–283 J/s or 1133 J/s = 550.3 J/s to 2200.3 J/s; (iii) the temperature rise in shearing, θ_s, is first calculated using the equation, $\theta_s = ((1-\beta).P_s)/\rho.c.v_{ac}.a_w$. However, to find β, we need to find R_T.tan φ using Boothroyd's relationship for β as a function of R_T.tan φ [25].

To calculate thermal number (R_T), we must know the density (ρ), thermal conductivity (k), and specific heat capacity (c) of G10530 steel. According to various property databases, ρ = 7700 kg/m^3, k = 54 J/smK, and c = 510 J/kgK. Therefore, R_T = (7700 kg/m^3 × 510 J/kgK × 250 m/min × 1/60 s/min × 0.1 × 10^{-3} m)/54 J/smK = 30.3. Owing to the fact that the working normal rake angle, γ_{ne}, is zero, tan φ = r_C. Thus, R_T.tan φ = 30.3 × 0.34 = 10.3. From Fig. 16, the value of β when R_T.tan φ = 10.3 is ~0.11. Now, $\theta_s = ((1-\beta).P_s)/\rho.c.v_{ac}.a_w$, where a_w is the width of cut = 10 mm (10 × 10^{-3} m). Therefore, θ_s = ((1–0.11) × (550.3 to 2200.3 J/s)/(7700 kg/m^3 × 510 J/kgK × 250 m/min × 1/60 s/min × 0.1 × 10^{-3} m × 10 × 10^{-3} m) = 29.9 °C to 119.7 °C, which is the mean variable temperature rise in the primary shear zone. The mean variable temperature rise in the secondary shear zone (frictional heat), $\theta_f = P_f/\rho.c.v_{ac}.a_w$ = (283 to 1133 J/s)/7700 kg/m^3 × 510 J/kgK × 160 m/min × 1/60 s/min × 0.1 × 10^{-3} m × 10 × 10^{-3} m) = 17.3 °C to 69.25 °C. The width of the secondary deformation zone divided by the chip thickness for unlubricated steel, γ = 0.2. The dimensionless length of the contact between chip and cutting tool (α_1) is stated by Boothroyd [20] to be the chip contact length (l_f) multiplied by the cutting ratio (r_C) divided by the chip thickness (a_o), i.e., $\alpha_1 = (l_f.r_C)/a_o$. For the present case, α_1 = (0.5 mm × 0.34)/0.296 mm = 0.574. Therefore, R_T/α_1 = 10.3/0.574 = 17.94. From Fig. 17, the value of θ_m/θ_f for γ = 0.2 is ~3. Hence, θ_m = 3 × (17.3 °C to 69.25)°C = 51.9 °C to 207.75 °C. The variable maximum temperature, $\theta_{max} = \theta_m + \theta_f + \theta_o$ = (51.9 to 207.75) + (17.3 to 69.25) + 22 = 91.2 °C to 299 °C, where θ_o is the room temperature.

According to Fig. 12 and at the start of cutting, the maximum temperature is computed to be ~300 °C, which is very close to the calculated value of 299 °C. The types of chips produced are short and blocky and are beneficial to the efficient operation of the boring process. The physical images of chips produced shown in Fig. 12 compare well with those predicted using the FE method.

5.3.3 Case 3 machining conditions—v_c = 160 m/min, n = 200 rpm, a_p = 0.1 mm, f_n = 0.35 mm/rev, Q = 5600 mm^3/min

The magnitude of force for the onset of chip formation varies between F_C ~ 200 N and 550 N (Fig. 13). The specific cutting pressure (energy consumed per unit volume of material removed), $p_s = F_C/A_O$, where F_C is the cutting force and A_O is the area of cut. The area of cut, A_O, is equal to the depth of cut multiplied by the length of cut, or A_O = 0.1 mm × 0.1 mm = 0.01 mm^2. When f_{edge}/t_r = 0.75, the variable specific cutting pressure, p_s, for chip formation is ~20 to 55 kN/mm^2.

The rate of energy consumption (heating rate) is given by the following equation: $W_C = F_C.v_C$, where v_C is the cutting speed. When f_{edge}/t_r = 0.75, the heating rate for chip formation is W_C ~ (200 to 550) N × 160 m/min × 1/60 s/min ~ 533 W to 1466 W. For chip formation conditions when f_{edge}/t_r = 0.75: (i) the rate of heat generated by friction between chip and cutting tool, $P_f = F_f.\ v_C.\ r_C$, where r_C is the chip thickness ratio and F_f is the friction force. For boring, $F_f = F_C$ because the working normal rake angle, γ_{ne}, is zero. CCR is the chip thickness divided by the uncut chip thickness, i.e., CCR = 0.296 mm/0.1 mm = 2.96. The chip thickness ratio, r_C = 0.1 mm/0.296 mm = 0.34. Therefore, P_f ~ (200 to 550) N × 160 m/min × 1/60 s/min × 0.34 ~ 181 J/s to 498.7 J/s; (ii) the rate of heat generation from shearing, $P_s = P_m$-P_f, or $P_s = (F_C.v_C)$-P_f. Thus, P_s = ((200 to 550) N × 160 m/min × 1/60 s/min)–181 J/s or 498.7 J/s = 352 J/s to 968 J/s; (iii) the temperature rise in shearing, θ_s, is first calculated using the equation, $\theta_s = ((1-\beta).P_s)/\rho.c.v_{ac}.a_w$. However, to find β, we need to find R_T.tan φ using Boothroyd's relationship for β as a function of R_T.tan φ [25].

To calculate thermal number (R_T), we must know the density (ρ), thermal conductivity (k), and specific heat capacity (c) of G10530 steel. According to various property databases, ρ = 7700 kg/m^3, k = 54 J/smK, and c = 510 J/kgK. Therefore, R_T = (7700 kg/m^3 × 510 J/kgK × 160 m/min × 1/60 s/min × 0.1 × 10^{-3} m)/54 J/smK = 19.39. Owing to the fact that the working normal rake angle, γ_{ne}, is zero, tan φ = r_C. Thus, R_T.tan φ = 19.39 × 0.34 = 6.59. From Fig. 16, the value of β when R_T.tan φ = 6.59 is ~0.16. Now, $\theta_s = ((1-\beta).P_s)/\rho.c.v_{ac}.a_w$, where a_w is the width of cut = 10 mm (10 × 10^{-3} m). Therefore, θ_s = ((1–0.16) × (352 to 968 J/s)/(7700 kg/m^3 × 510 J/kgK × 160 m/min × 1/60 s/min × 0.1 × 10^{-3} m × 10 × 10^{-3} m) = 28.24 °C to 77.66 °C, which is the mean variable temperature rise in the primary shear zone. The mean variable temperature rise in the secondary shear zone (frictional heat) is given by the following equation: $\theta_f = P_f/\rho.c.v_{ac}.a_w$ = (181 to 498.7 J/s)/7700 kg/m^3 × 510 J/kgK × 160 m/min × 1/60 s/min × 0.1 × 10^{-3} m × 10 × 10^{-3} m) = 17.28 °C to 47.62 °C. The width of the secondary deformation zone divided by the chip thickness, γ = 0.2 for unlubricated steel. The dimensionless length of the contact between chip and cutting tool (α_1) is stated by Boothroyd [20] to be the chip contact length (l_f) multiplied by the cutting ratio (r_C) divided by the chip thickness (a_o), i.e., $\alpha_1 = (l_f.r_C)/a_o$. For the present case, α_1 = (0.5 mm × 0.34)/0.296 mm = 0.574. Therefore, R_T/α_1 = 19.39/0.574 = 33.78. From Fig. 17, the value of θ_m/θ_f for γ = 0.2 is ~3.9. Hence, θ_m = 3.9 × (17.28 °C to 47.62) °C = 67.4 °C to 185.7 °C. The variable maximum temperature, $\theta_{max} = \theta_m + \theta_f + \theta_o$ = (67.4 to 185.7) + (17.28 to 47.62) + 22 = 106.7 °C to 255.3 °C, where θ_o is the room temperature.

According to Fig. 14 and at the start of cutting, the maximum temperature is computed to be ~200 °C, which is very close to the calculated value of 255.3 °C. The types of chips produced are short and blocky and are beneficial to the efficient operation of the boring process. The physical images of chips produced shown in Fig. 14 compare well with those predicted using the FE method.

6 Conclusions

The aim of the study was to predict the conditions of machining that would contribute to the fracturing of chips generated from the machining of G10530 axle hub turnings. The use of commercially available Langrangian-Euler formulated FE method coupled with a power law material model that adaptively re-meshes during the simulation of machining conditions, predicted that when using variable cutting speeds, long chips will fragment into short chips, thus eliminating chip build-up (or crowding of rotating machine parts with cut chips). In practice, the replacement of the old method of machining with the new method of varying cutting speeds produces much smaller chips as predicted by the FE method and demonstrated physically be the generation of short chips (Figs. 11, 13, and 15). The rectification of machining parameters to produce smaller chips does not necessitate the use of complex chip breaker geometry, thus reducing tooling costs by using plain inserts. From this study, the following conclusions are drawn:

1. Short chips can be created using variable cutting speeds but it is noted that this method will affect the quality of the surface generated on the axle hub housing;
2. The FE method can be used to analyze chip formation in order to optimize machining conditions for the turning of G10530 axle hub housings in order to produce productive chip formations;
3. For the current practice of machining axle hub housings, when f_{edge}/t_r = 0.25, the level of power required for chip formation is calculated to be 6400 W generating a calculated maximum temperature at the onset of chip formation to be ~563 °C (FE computed value is ~600 °C), and when f_{edge}/t_r = 0.75, the level of power required for chip formation is calculated to be 3200 W generating a calculated maximum temperature at the onset of chip formation to be ~292 °C (FE computed value is ~300 °C). Therefore, under current practice conditions, it is better to use a cutting tool with a large edge radius in order to reduce the amount of power required to form chips. Larger edge radii also reduce maximum temperature generated at the contact zone;
4. When forming chips at variable cutting speeds and a large cutting edge radius tool (f_{edge}/t_r = 0.75), the best case conditions are one that draw the least power and generate the lowest temperature at the chip-tool interface. Therefore, the following machining conditions should be used: v_c = 160 m/min, *n* = 200 rpm, a_p = 0.1 mm, f_n = 0.35 mm/rev, Q = 5600 mm^3/min. These conditions draw between 533 W and 1600 W of power during chip formation with a maximum interface temperature of ~255 °C (FE computed value is ~200 °C).
5. The experimental methods developed by Boothroyd [25] appear to describe the machining conditions at the steady state very accurately. However, after the onset of stable machining conditions, the FE method tends to generate more accurate values that describe the conditions of unsteady chip formation under variable cutting speed conditions.

References

1. Yeoman IF (1922) Turret lathe tooling: equipment for machining differential gear housings on Foster turret lathes. Machinery 28: 356–358. Published by the Industrial Press, Edited by Lester Gray French, January 1922, New York, USA
2. Gomes da Sousa JA, Nasciento da Sousa M, Jackson MJ, Machado AR (2014) Comparison of the machining performance of new and Re-ground cemented carbide drills machining steel. Proceedings of the Institution of Mechanical Engineers (London) – Part B: Journal of Engineering Manufacture 228:376–387
3. Santos MC, Machado AR, Barrozo MAS, Jackson MJ, Ezugwu EO (2015) Multiobjective optimization of cutting conditions when turning 1350-O and 7075-T6 aluminum alloys using genetic algorithms. Int J Adv Manuf Technol 76:1123–1138
4. Schmidt P, Handy RG, Anderson T, Rees T, Morrell JS, Williams W, Jackson MJ (2016) Residual surface stress: comparing traditional and modulated tool path machining processes. Mater Sci Technol 32(14):1471–1483
5. Ziberov M, da Silva MB, Jackson MJ, Hung WP (2016) Effect of cutting fluid in Micromilling of Ti-6Al-4V titanium alloy. Procedia Manufacturin 5:332–347
6. da Silva LC, da Mota PR, da Silva MB, Sales WF, Machado AR, Jackson MJ (2016) Burr height minimization using the response surface methodology in milling of PH 13-8Mo stainless steel. Int J Adv Manuf Technol 87:3485–3496
7. Johnson GR, Cook WH (1983) 'a constitutive model and data for metals subjected to large strains, high strain rates and high temperatures'. Proceedings of the 7th international symposium on ballistics. The Hague, pp 541–547
8. Guo YB, Wen Q, Hortemeyer MF (2005) An internal state variable plasticity-based approach to determine dynamic loading history effects on material property in manufacturing processes. Int J Mech Sci 47:1423–1441
9. Seo S, Min O, Yang H (2005) Constitutive equation for Ti-6Al-4V at high temperatures measured using the SHPB technique. International Journal of Impact Engineering 31:735–754
10. Calamaz M, Coupard D, Girot F (2008) A new material model for 2D numerical simulation of serrated chip formation when machining titanium alloy Ti-6Al-4V. International Journal of Machine Tools & Manufacture 48:275–288
11. Sheikh-Ahmadn JY, Bailey JA (1995) A constitutive model for commercially pure titanium. ASME Journal of Engineering Materials and Technology 117:139–144
12. Zerilli FJ, Armstrong RW (1986) Dislocation-mechanics-based constitutive relations for material dynamics calculation. J Appl Phys 61:1816–1827
13. Abed FH, Voyiadjis GZ (2005) A consistent modified Zerilli-Armstrong flow stress model for BCC and FCC metals for elevated temperatures. Acta Mech 175:1–18
14. Third Wave AdvantEdge™ User's Manual Version 5.2 (2008) Third wave systems. Minneapolis
15. Silin SS (1979) 'similarity methods in metal cutting' (in Russian). Mashinostroenie, Moscow
16. Astakhov VP (1999) Metal cutting mechanics. CRC Press, Boca Raton
17. Astakhov VP, Xiao X (2008) A methodology for practical cutting force evaluation based on the energy spent in the cutting system. Mach Sci Technol 12:325–347
18. Astakhov VP, Shvets S (2004) The assessment of plastic deformation in metal cutting. J Mater Process Technol 146:193–202
19. Astakhov VP, Outeiro JC (2008) Metal cutting mechanics - finite element modelling. In: Davim JP (ed) Machining fundamentals and recent advances. Springer, London, pp 1–27
20. Carslaw HS, Jaeger JC (1959) Conduction of heat in solids, 2nd edn. Oxford University Press, Oxford
21. Poletica MF (1969) Contact loads on cutting tool interface surfaces. Mashinostroenie, Moscow
22. Boothroyd G (1975) Fundamentals of metal machining and machine tools. Scripta-McGraw Hill, London
23. Chandiramani KG (1975) Metal cutting technology and experiments. McGraw-Hill, New Delhi
24. Coromant S (2010) Metal cutting technology—technical guide. Elanders Press, Stockholm
25. Boothroyd G (1963) Temperatures in orthogonal metal cutting. Proceedings of the Institution of Mechanical Engineers 177:789–810